Canonical Wnt Signaling and the Regulation of Divergent Mesenchymal Fgf8 expression in Axolotl Limb Development and Regeneration

Giacomo L. Glotzer[1,3], Pietro Tardivo[1,2,3]*, Elly M. Tanaka[1]*

[1] Research Institute of Molecular Pathology (IMP), Vienna BioCenter (VBC), Campus-Vienna-Biocenter 1, 1030 Vienna, Austria
[2] Vienna BioCenter PhD Program, Doctoral School of the University of Vienna and Medical University of Vienna, A-1030, Vienna, Austria
[3] Equal contribution
*Corresponding

Abstract

The expression of Fibroblast growth factors (Fgf) ligands in a specialized epithelial compartment, the Apical Ectodermal Ridge (AER), is a conserved feature of limb development across vertebrate species. In vertebrates, *Fgf 4, 8, 9,* and *17* are all expressed in the AER. An exception to this paradigm is the salamander (axolotl) developing and regenerating limb, where key Fgf ligands are expressed in the mesenchyme. The mesenchymal expression of Amex.*Fgf8* in axolotl has been suggested to be critical for regeneration. To date, there is little knowledge regarding what controls Amex.*Fgf8* expression in the axolotl limb mesenchyme. A large body of mouse and chick studies have defined a set of transcription factors and canonical Wnt signaling as the main regulators of epidermal *Fgf8* expression in these organisms. In this study, we address the hypothesis that alterations to one or more of these components during evolution has resulted in mesenchymal Amex.*Fgf8* expression in the axolotl. To sensitively quantify gene expression with spatial precision, we combined optical clearing of whole-mount axolotl limb tissue with single molecule fluorescent *in situ* hybridization and a semi-automated quantification pipeline. Several candidate upstream components were found expressed in the axolotl ectoderm, indicating that they are not direct regulators of Amex.*Fgf8* expression. We found that Amex.*Wnt3a* is expressed in axolotl limb epidermis, similarly to chicken and mouse. However, unlike in amniotes, Wnt target genes are activated preferentially in limb mesenchyme rather than in epidermis. Inhibition and activation of Wnt signaling results in downregulation and upregulation of mesenchymal Amex.*Fgf8* expression respectively. These results implicate a shift in tissue responsiveness to canonical Wnt signaling from epidermis to mesenchyme as one step contributing to the unique mesenchymal Amex.*Fgf8* expression seen in the axolotl.

Introduction

Signaling mediated by members of the Fibroblast Growth Factor family is necessary for normal limb development and for limb regeneration in the salamander *Ambystoma mexicanum* (axolotl), a primary model for regeneration research (Nacu, Gromberg et al. 2016, Purushothaman, Elewa et al. 2021). In less-regenerative tetrapods, like mouse (*Mus musculus*), Fgf signaling is similarly required for limb development (Lewandoski, Sun et al. 2000, Moon and Capecchi 2000, Sun, Mariani et al. 2002, Mariani, Ahn et al. 2008). In mammals, *Fgfs 4, 8, 9* and *17* are produced by cells in the apical ectodermal ridge (AER), a thickened epidermal structure at the distal dorso-ventral boundary of the limb bud. Fgf signals from the AER act on the underlying mesenchyme to sustain its growth and patterning. Of the AER Fgfs, Mmu.*Fgf8* is the only one that is individually required for normal limb development in mice (Mariani, Ahn et al. 2008).

Limb regeneration in the axolotl proceeds through the formation of the blastema, a structure that resembles the limb bud, both at the morphological and transcriptional level. In both the axolotl limb blastema and limb bud, Amex.*Fgfs 8, 9 and 17* are expressed in the mesenchymal compartment, unlike in other vertebrates, while Amex.*Fgf4* transcription is negligible or absent (Christensen, Weinstein et al. 2002, Nacu, Gromberg et al. 2016, Purushothaman, Elewa et al. 2021). Restriction of Amex.*Fgf8* expression to the mesenchymal compartment is to our knowledge unique to the salamander limb, where it serves a crucial role in connecting positional identity with growth and patterning during limb regeneration. Nacu et. al. showed that Amex.*Fgf8* expression is restricted to the anterior mesenchyme of the regenerating blastema, while cells of the posterior blastema mesenchyme do not express Amex.*Fgf8* (Nacu, Gromberg et al. 2016). When a limb amputation is performed, anterior cells express Amex.*Fgf8* and posterior cells express Amex.*Shh,* initiating a positive feedback loop in which Amex.*Fgf8* and Amex.*Shh* reciprocally maintain each other's expression: prolonged expression of both signaling molecules sustains blastema growth and limb regeneration. The anterior mesenchymal expression of Amex.*Fgf8* therefore mediates the communication between anterior and posterior cells in the blastema. The incompetence of other blastema cells to transcribe Amex.*Fgf8* acts as a safeguard to restrict the initiation of blastema formation to injuries involving both anterior and posterior limb cells. It is interesting to note that the positive feedback relationship between *Fgfs* and *Shh* was initially described in the mammalian limb, between *Shh* in the posterior mesenchyme and *Fgf8* in the epidermis (Laufer, Nelson et al. 1994, Niswander, Jeffrey et al. 1994). Expression of Amex.*Fgf8* in the mesenchyme could serve to couple limb outgrowth with anterior-posterior positional information, a capacity that is restricted to mesenchymal cells in the axolotl (Carlson 1975).

Given the interesting role mesenchymal Amex.*Fgf8* expression plays in axolotl limb regeneration, we asked: how has the axolotl limb signaling network been rewired to elicit this adaptation? In the mouse limb bud AER, expression of Mmu.*Fgf8* is controlled at the genetic level by a set of enhancers proximal to the gene locus (Marinic, Aktas et al. 2013). Kawaguchi et. al. recently determined that conserved orthologs of the majority of these enhancers are present in the axolotl genome, and that at least one of these drives expression of a reporter construct in the mesenchyme of the axolotl limb (Schloissnig, Kawaguchi et al. 2021). This suggests that changes at the level of trans-acting factors may determine the divergent expression of Amex.*Fgf8* in the axolotl limb.

Transcription factors and intercellular signaling molecules that regulate AER-associated *Fgf8* expression have been identified in chicken (*Gallus gallus*) and mouse. In mice, AER expression of Mmu.*Fgf8* has been shown to be dependent on mesenchymal Mmu.*Fgf10* acting through the epidermis-specific receptor isoform Mmu.*Fgfr2b* (Xu, Weinstein et al. 1998, De Moerlooze, Spencer-Dene et al. 2000, Zhang, Ibrahimi et al. 2006, Sekine, Ohuchi et al. 2019). Using the chick model, it was established that Gga.*Fgf10* induces epidermal expression of the canonical Wnt ligand Gga.*Wnt3a*. *Wnt3a* (chick) and *Wnt3* (mouse), together with BMPR1a dependent signaling, activate canonical Wnt signaling within AER cells to induce *Fgf8* (Kengaku, Capdevila et al. 1998, Kawakami, Capdevila et al. 2001, Barrow, Thomas et al. 2003). In mice, genetic removal of epidermal Mmu.*Wnt3* or the canonical Wnt signaling effector ß-catenin is sufficient to abolish Mmu.*Fgf8* expression in the limb, while expression of a constitutively active ß-catenin markedly expands the Mmu.*Fgf8* expression domain and induces ectopic Mmu.*Fgf8* expression in the dorsal and ventral epidermis (Barrow, Thomas et al. 2003, Soshnikova, Zechner et al. 2003). Furthermore, mesenchymal expression of a constitutively active ß-catenin construct appeared to potentially induce sporadic mesenchymal expression of Mmu.*Fgf8* (Hill, Taketo et al. 2006). Similarly in the chick developing limb, misexpression of ß-catenin, Gga.*Wnt3a* or the Wnt transcription factor Gga.*Lef1* is sufficient to induce Gga.*Fgf8* expression ectopically in the dorsal and ventral epidermis (Kengaku, Capdevila et al. 1998). In addition to Wnt signaling components, Buttonhead transcription factors *Sp8* and *Sp6* have also been shown to be necessary for *Fgf8* expression and act downstream of canonical Wnt signaling in the mammalian limb (Kawakami, Esteban et al. 2004, Talamillo, Delgado et al. 2010, Lin, Yin et al. 2013, Haro, Delgado et al. 2014). Finally, Dlx factors *Dlx5* and *Dlx6* have been implicated in the maintenance of the AER and are required to sustain *Fgf8* expression, but are dispensable for its induction (Robledo, Rajan et al. 2002).

Little is known about the Amex.*Fgf8* regulatory machinery in the axolotl limb. Amex.*Fgf10* is expressed in the mesenchyme, along with *Fgfs 8, 9* and *17* (Christensen, Weinstein et al. 2002, Nacu, Gromberg et al. 2016, Purushothaman, Elewa et al. 2021). This challenges the epithelial-mesenchymal interaction model of the mammalian and avian limb where mesenchymal *Fgf10* and epidermal *Fgf8* reciprocally sustain each other's expression acting on different, tissue-specific, receptor isoforms. A recent publication reported that no Fgf receptor is expressed in the axolotl epidermis (Purushothaman et al., 2019), suggesting that the epidermal side of the interaction may be completely absent. This is at odds with previous studies that showed *Fgfr2b* expression in the basal epidermis of the newt blastema (Poulin and Chiu 1995). The expression domain of Amex.*Wnt3* ligands, the major *Fgf8* AER regulators, has not been determined in the axolotl limb although Wnt3a expression is present in the salamander limb blastema as determined by qPCR (Singh, Doyle et al. 2012). Another canonical Wnt ligand, Amex.*Wnt10* was found in similar amounts in lateral injuries (surface wounds that do not trigger regeneration) and limb amputations, suggesting its role may be restricted to wound response (Knapp, Schulz et al. 2013). Multiple studies reported that chemical activation of the canonical Wnt pathway increases cell proliferation in the salamander regenerating blastema (Singh, Doyle et al. 2012, Wischin, Castaneda-Patlan et al. 2017) but it has not been elucidated if the main site of canonical Wnt signaling activity is the blastema epidermis or mesenchyme. Although overexpression of the Wnt antagonist *Axin1* is sufficient to block limb development and regeneration in the axolotl (Kawakami, Rodriguez Esteban et al. 2006), it is unclear if this effect is mediated through downregulation of Amex.*Fgf8*. In the axolotl limb, it has also not been determined whether the transcription factors Amex.*Sp6*, Amex.*Sp8*, Amex.*Dlx5*, Amex.*Dlx6* and Amex.*Lef1* display mesenchymal or epidermal expression, nor if their function in regulating Amex.*Fgf8* is conserved.

Despite the expression of Fgf ligands in the mesenchymal compartment, classical experiments have shown that the epidermis of the axolotl blastema is necessary for both initial accumulation and proliferation of cells in the blastema (Thornton 1957, Campbell and Crews 2008). For example, Axolotl MARCKS like Protein has been identified as an epidermal factor that induces the initial proliferation response in the blastema (Sugiura, Wang et al. 2016). Recent single cell studies have highlighted that different cell populations are present in the regenerating axolotl epidermis (Leigh, Dunlap et al. 2018, Rodgers, Smith et al. 2020, Li, Wei et al. 2021), and previous studies have indicated that the basal layer of the axolotl epidermis expresses some markers of the mammalian AER, including fibronectin and Amex.*Dlx3* (Christensen and Tassava 2000).

In this study we take advantage of published single cell RNA sequencing (scRNA seq) datasets for the axolotl limb bud (Lin, Gerber et al. 2021) and blastema (Li, Wei et al. 2021) to elucidate the tissue compartment specificity of candidate Amex.*Fgf8* regulators. To precisely visualize tissue transcripts in the anatomical complexity of the developing and regenerating axolotl limb, we further develop a protocol that combines HCR *in situ* hybridization (Choi, Schwarzkopf et al. 2018) with Ce3D tissue clearing (Li, Germain et al. 2017, Li, Germain et al. 2019) and light sheet imaging. We then implemented semi-automated image analysis pipelines to quantitatively compare transcript abundances in different tissue compartments and upon pharmacological perturbation.

We identify conserved and divergent features of the axolotl limb signaling network and implicate enhanced canonical Wnt signaling in the axolotl limb mesenchyme as one of the regulators of Amex.*Fgf8* mesenchymal expression.

Results

Expression of Transcription Factors Known to Regulate *Fgf8* in the Chick and Mouse AER

Several transcription factors have been functionally linked with the induction or maintenance of *Fgf8* in the mammalian AER (Zuniga and Zeller 2020). To determine whether these transcription factors are potentially upstream of axolotl Amex.*Fgf8*, we investigated if they are expressed in the epidermis and/or mesenchyme in the axolotl developing and regenerating limb. To this end, we first analyzed published scRNA seq datasets for the axolotl stage 52 axolotl hindlimb bud (Lin, Gerber et al. 2021) and 7 days-post-amputation axolotl forelimb blastema (Li, Wei et al. 2021). Both single cell datasets were reanalyzed to match the latest axolotl transcriptome annotation (Schloissnig, Kawaguchi et al. 2021) and re-clustered, using known markers for cluster assignment (Supp. Fig. 1, 2). We then used HCR *in situ* hybridization in tissue sections and whole-mount cleared limb preparations of forelimb buds and blastemas of comparable stages (stage 45-46 forelimb bud, 7 days post amputation forelimb blastema) to validate the expression domains and acquire spatial information. To achieve precise visualization of transcripts in the anatomical complexity of the entire axolotl developing and regenerating limb, we combined HCR *in situ* hybridization with Ce3D tissue clearing and light sheet imaging (see Materials and Methods).

Buttonhead transcription factors Mmu.*Sp6* and Mmu.*Sp8* are expressed in the AER of the mouse developing limb, and their knockout abolishes Mmu.*Fgf8* expression (Lin, Yin et al.

2013, Haro, Delgado et al. 2014). Analysis of scRNA seq data from the axolotl limb bud and blastema (Li, Wei et al. 2021, Lin, Gerber et al. 2021) revealed expression of Amex.*Sp6* and Amex.*Sp8* in the epidermis and not in mesenchyme (Fig. 1A, 1A', 1B, 1B'). We performed whole mount HCR staining in regenerating axolotl limb blastemas and limb buds (Fig. 2B, 2B') and confirmed that Amex.*Sp6* is expressed in the epidermis of the axolotl limb bud and regenerating blastema. Interestingly, we detected Amex.*Sp6* also in the mesenchyme of the axolotl limb bud, in a domain proximal to Amex.*Fg8* expression (Supp. Fig. 3). This proximal mesenchymal expression of Amex.*Sp6* was absent in the blastemas that we analyzed and is unlikely to regulate the more distal Amex.*Fg8* expression in the axolotl limb bud. Using HCR in situ hybridization, we then found that Amex.*Sp8* is exclusively expressed in the epidermis (Fig. 2C, 2C'), with a strong enrichment in the basal layer (the inner layer facing the mesenchyme) in both the axolotl and limb bud and blastema. This indicates that buttonhead factors are unlikely to directly regulate Amex.*Fgf8* expression in the mesenchyme and that the lack of Amex.*Fgf8* expression in the axolotl epidermis is not due to the absence of these factors.

Dlx factors Mmu.*Dlx5* and Mmu.*Dlx6* are also expressed in the mouse AER, where they function to maintain Mmu.*Fgf8* expression (Robledo, Rajan et al. 2002). Single cell analysis of the axolotl blastema and limb bud detected transcripts in both the epidermal and mesenchymal compartments (Fig. 1C, 1C', 1D ,1D'). Whole-mount HCR staining revealed that expression of Amex.*Dlx5* is enriched in the distal mesenchyme and in the basal epidermis of the blastema (Fig. 2D) and limb bud (Fig. 2D'). Expression of Amex.*Dlx5* in the limb epidermis suggests that in the axolotl, similarly to the mouse, Amex.*Dlx5* is not sufficient to induce Amex.*Fgf8* expression. The strong mesenchymal Amex.*Dlx5* expression distinguishes the axolotl limb from the mammalian one and could be consistent with a conserved role in maintaining Amex.*Fgf8* expression.

The canonical Wnt pathway is a main regulator of *Fgf8* expression in the chicken and mouse developing limb. In the chick, the Wnt transcription factor Gga.*Lef1* is required for AER Gga.*Fgf8* expression. Furthermore, Gga.*Lef1* overexpression is sufficient to induce ectopic Gga.*Fgf8* expression in the non-AER epidermis (Kengaku, Capdevila et al. 1998). In mouse, the double knockout of the Wnt transcription factors Mmu.*Lef1* and Mmu.*Tcf1* abolishes AER Mmu.*Fgf8* expression (Galceran, Farinas et al. 1999). In our scRNA seq analysis, we could detect expression of Amex.*Lef1* in both epidermal and mesenchymal cells (Fig. 1E, 1E'). Using HCR, we found that Amex.*Lef1* is expressed broadly in the limb bud and blastema mesenchyme (Fig. 2E, 2E'). We also detected expression in the limb bud and blastema epidermis, strongest in the distal portion of the basal epidermis (Fig. 2E, 2E'). Considering that overexpression of Gga.*Lef1* in chick is sufficient to induce ectopic Gga.*Fgf8* expression (Kengaku, Capdevila et al. 1998) , we note here that, at least at the levels observed, it is not sufficient to allow Amex.*Fgf8* expression in the axolotl limb epidermis. The broad expression pattern of Amex.*Lef1* in the axolotl limb mesenchyme could be compatible with a role in inducing or maintaining mesenchymal Amex.*Fgf8* expression in axolotl.

Our analysis revealed that the transcription factors Amex.*Sp8,* Amex.*Sp6,* Amex.*Dlx5,* Amex.*Dlx6* and Amex.*Lef1* are expressed in the axolotl developing and regenerating limb epidermis, in particular all are present in the basal epidermis. This indicates that, in the axolotl limb epidermis, the combined endogenous expression of these factors is not sufficient to activate Amex.*Fgf8* transcription. While expression of Sp factors appeared uniquely epidermal, Amex.*Dlx5,* Amex.*Dlx6* and Amex.*Lef1* are expressed in the limb bud and

blastema mesenchyme, leaving open the possibility that they have a role in the regulation of Amex.*Fgf8* expression in this tissue compartment.

Conserved and divergent expression of canonical Wnt pathway components and upstream regulators

Canonical Wnt signaling controls AER-associated *Fgf8* expression and mediates the communication between the epidermal and mesenchymal limb compartments in chick and mouse. To verify if this interaction is conserved in axolotl, we decided to investigate the expression of the canonical Wnt3 ligands and of the components that are known to induce their expression in the mammalian limb bud AER, primarily *Fgf10* and its receptor *Fgfr2b*. We furthermore profiled *Rspo2*, an extracellular potentiator of Wnt signaling that is necessary for normal limb development (Xu, Weinstein et al. 1998, De Moerlooze, Spencer-Dene et al. 2000, Zhang, Ibrahimi et al. 2006, Sekine, Ohuchi et al. 2019). Finally, to localize the site of canonical Wnt signaling, we examined the expression of *Axin2*, a target of the canonical Wnt pathway that is often used as a readout of signaling activation strength (Nam, Park et al. 2007, Itou, Taniguchi et al. 2011, Eckei, Boing et al. 2016, Nusse and Clevers 2017).

Conserved gene expression features

In both blastema and limb bud scRNA seq datasets we detected Amex.*Fgf10* transcripts in the mesenchymal cluster (Fig. 3A, 3A'), consistent with previous reports (Christensen, Weinstein et al. 2002, Nacu, Gromberg et al. 2016, Purushothaman, Elewa et al. 2021). Using HCR *in situ* hybridization we confirmed strong and broad mesenchymal expression (Fig. 4B, 4B'). Surprisingly, we additionally found Amex.*Fgf10* transcripts in a small and distinct cell population located in the basal layer of the distal epidermis. To exclude that this population is of mesenchymal origin we performed HCR *in situ* hybridization and lineage tracing using *Prrx1*-Cre transgenic axolotls (Supp. Fig. 4) (Gerber, Murawala et al. 2018). During mammalian limb development, mesenchymal *Fgf10* signals to the epidermis via the specific receptor isoform *Fgfr2b* (Xu, Weinstein et al. 1998, De Moerlooze, Spencer-Dene et al. 2000, Zhang, Ibrahimi et al. 2006, Sekine, Ohuchi et al. 2019). In the axolotl, using HCR, we detected Amex.*Fgfr2b* transcripts through the entire basal epidermis of the blastema (Fig. 4C) and limb bud (Fig. 4C'), consistent with Amex.*Fgf10* signaling to the epidermis as in other vertebrates.

Fgf10 signaling is thought to be required for expression of Mmu.*Wnt3* in mouse and Gga.*Wnt3a* in chick. We therefore assessed expression of both Amex.*Wnt3* and Amex.*Wnt3a*: we found Amex.*Wnt3a* transcripts in the epidermal cluster (Fig. 3B, 3B'), while we could only detect negligible Amex.*Wnt3* transcripts in any cell type. HCR data confirmed that Wnt3a expression is present in the axolotl limb bud and blastema basal epidermis (Fig. 4D, 4D'). These results suggest that the epidermal induction of Amex.*Wnt3a* is downstream of mesenchymal Amex.*Fgf10* signaling in the axolotl limb as in mouse.

Wnt signaling activity and the Rspo2 co-activator show divergent gene expression features

In mouse and chick limb development, epidermal signaling from Mmu.*Wnt3* or *Gga.Wnt3a* is considered to induce canonical Wnt signaling in the AER (Xu, Weinstein et al. 1998, De Moerlooze, Spencer-Dene et al. 2000, Zhang, Ibrahimi et al. 2006, Sekine, Ohuchi et al. 2019). This signal activation results in strong AER expression of *Axin2*, a canonical Wnt target that is often used to determine pathway activity (Nam, Park et al. 2007, Itou, Taniguchi et al. 2011, Eckei, Boing et al. 2016, Nusse and Clevers 2017). *Wnt3* ligands act also on the

underlying mesenchyme, where they induce expression of *Axin2*, albeit at lower levels (Kengaku, Capdevila et al. 1998).

To determine the prevalent site of canonical Wnt signaling in the axolotl limb, we evaluated the expression of Amex.*Axin2*. Single cell analysis indicated that Amex.*Axin2* expression in the axolotl limb is biased towards the mesenchymal compartment (Fig. 3C, 3C'). Using whole-mount HCR, we confirmed strong expression in the mesenchyme, with a distal and sub-epidermal enrichment in both the axolotl blastema (Fig. 4D, 4E) and limb bud (Fig. 4D', 4E'). Epidermal expression is also present, but weaker. The mesenchymal enrichment in Amex.*Axin2* expression distinguishes the axolotl limb from the mammalian one.

Mmu.*Rspo2*, a secreted ligand that acts as an enhancer for Wnt signaling, is expressed in the mouse limb AER where it functions to potentiate canonical Wnt signaling activity. Mutations in the *Rspo2* gene cause severe limb truncations in mice, and complete loss of limbs in humans (Nam, Park et al. 2007, Aoki, Kiyonari et al. 2008, Bell, Schreiner et al. 2008, Yamada, Nagao et al. 2009, Szenker-Ravi, Altunoglu et al. 2018). Our single cell analysis revealed that Amex.*Rspo2* expression is absent from the axolotl developing and regenerating limb epidermis but present in the mesenchyme (Fig. 3D, 3D'). We confirmed the strictly mesenchymal expression of Amex.*Rspo2* using HCR (Fig. 4E, 4E'). In both the axolotl limb bud and blastema, mesenchymal Amex.*Rspo2* expression is biased along the dorso-ventral axis, suggesting a possible role in dorsoventral limb patterning (Supp. Fig. 5).

Amex.*Fgf8* expression is responsive to pharmacological perturbation of Wnt signaling

The mesenchymal enrichment of Amex.*Axin2* transcripts prompted us to test if canonical Wnt signaling regulates Amex.*Fgf8* expression in the mesenchyme of the axolotl regenerating limb, and whether enhancing Wnt signaling in the epidermis would be sufficient to induce ectopic Amex.*Fgf8* expression. To this end, we treated regenerating axolotls with a chemical Wnt agonist or antagonist and used HCR in whole-mount blastema samples to visualize the effect on transcription of Amex.*Fgf8*, using Amex.*Axin2* as a readout for successful pathway perturbation. To accurately evaluate the effect of the drug treatments, we developed a semi-automated image analysis pipeline that enables the segmentation of gene expression domains, the removal of the signal derived from auto-fluorescent blood cells in the blastema, and the quantitative comparison of gene expression levels (materials and methods, Supp. Fig. 6).

First, to assess the possible role of Wnt signaling in maintaining Amex.*Fgf8* expression, we performed drug treatments in regenerating blastemas. Axolotls were amputated at mid-zeugopod level, allowed to form a blastema over 5 days and then were bathed for 12 hours in a 25µM solution of IWR-1-endo (Sigma), an inhibitor of the canonical Wnt pathway that acts by stabilizing Axin2 and consequently increasing the degradation of ß-catenin. IWR treatment induced a similar decrease in Amex.*Axin2* and Amex.*Fgf8* transcripts when compared to DMSO-treated controls (Fig. 5A, 5B), suggesting that canonical Wnt signaling is required to sustain expression of Amex.*Fgf8* in the axolotl blastema mesenchyme.

Second, to assess whether canonical Wnt signaling can promote Amex.*Fgf8* expression, axolotl with 5 days blastemas were bathed in a solution of 50 µM CHIR-99021 (Sigma) or in DMSO control for 3, 6 and, in a separate experiment, 12 hours. As expected, Amex.*Axin2* expression was upregulated in all CHIR treatment conditions compared to controls (Fig. 5C).

After 3 hours of CHIR treatment, expression of Amex.*Fgf8* was significantly upregulated (Fig. 5D). By 6 hours, we found that Amex.*Fgf8* was not significantly different in CHIR-treated and untreated samples while after 12 hours Amex.*Fgf8* expression levels were significantly decreased when compared to control samples (Fig. 5D).

Amex.*Fgf8* transcripts, although upregulated after 3h of CHIR treatment, were always present exclusively in the native Amex.*Fgf8* domain in the anterior blastema mesenchyme (Supp. Fig. 7). Our results are consistent with canonical Wnt signaling regulating Amex.*Fgf8* expression in the anterior mesenchyme. Interestingly, while we observe a Wnt-induced upregulation of Amex.*Fgf8* in the anterior mesenchyme, Wnt activation is not sufficient to induce ectopic Amex.*Fgf8* expression in the posterior mesenchyme nor in the epidermis indicating regulation of Amex.*Fgf8* by other, yet unidentified factors. Surprisingly, we observed that in all treatment conditions Amex.*Axin2* expression retained a strong mesenchymal bias, suggesting that the axolotl epidermis may be partially refractory to canonical Wnt signaling activation. To verify this, we quantified the increase in Amex.*Axin2* in the mesenchymal and epidermal compartments after 3 and 6 hours of CHIR treatment and found that upregulation of Amex.*Axin2* is present in both compartments, but stronger in the mesenchyme (Fig 5E, Supp. Fig. 8).

Discussion

Salamanders are the sole modern tetrapod capable of regenerating their limbs throughout their lifespans. Along with a remarkable regenerative ability, the salamander limb presents other distinctive features in its development, both at the morphological and molecular level. The digital elements are formed in an anterior to posterior order, contrary to other species (Shubin NH 1986, Nye, Cameron et al. 2003, Frobisch, Bickelmann et al. 2015, Purushothaman, Elewa et al. 2021). Furthermore, key molecular players of limb development, such as Fgf ligands *Fgf 8, 9*, and *17*, exhibit divergent expression in salamander limb development and regeneration when compared to mouse and chick (Nacu, Gromberg et al. 2016, Purushothaman, Elewa et al. 2021) .

We have focused on the unique mesenchymal expression of Amex.*Fgf8* with the aim of establishing how the upstream signaling circuit characterized in amniotes differs in axolotl. We found that most of the components that act upstream of mammalian *Fgf8* expression in the AER are present in the axolotl epidermis, with an enrichment in the most basal layer. These include Amex.*Fgfr2b*, the receptor for *Fgf10*, Amex.*Wnt3a* and the transcription factors Amex.*Sp8*, Amex.*Sp6*, Amex.*Dlx5*, Amex.*Dlx6* and Amex.*Lef1*. Expression of these components in the axolotl epidermis is evidently insufficient to induce expression of Amex.*Fgf8* in epidermis. This deficit could be explained by the acquisition of completely new and different regulators of Amex.*Fgf8* in the axolotl limb, or by the presence of components that repress Amex.*Fgf8* expression in the axolotl epidermis, or by the lack of a different necessary regulator that may be present in the mouse epidermis but absent in the axolotl epidermis. Epidermal expression of Amex.*Fgfr2b* and Amex.*Wnt3a* suggests that in the axolotl limb, like in the mouse and chick limb, Amex.*Fgf10* signals to the epidermis to induce the expression of a canonical *Wnt3* ligand. There are slight differences in the epidermal pattern of expression of *Wnt3* ligands between the chick and mouse limb: in chick Gga.*Wnt3a* expression is restricted to the AER (Kawakami, Capdevila et al. 2001), while in mouse Mmu.*Wnt3* expression is present in the entire limb epidermis (Barrow, Thomas et al. 2003). Nevertheless, it has been speculated that in both species, Mmu.*Wnt3/*Gga.*Wnt3a* ligands signal to induce strong Wnt signaling activation specifically in the AER, a cell type

that has an enhanced sensitivity to canonical Wnt signaling (Kengaku, Capdevila et al. 1998, Barrow, Thomas et al. 2003). In the axolotl, unlike the mouse, we found that a discrete epidermal compartment exhibiting high activity of the canonical Wnt pathway is absent, while strong canonical Wnt pathway activity appears to be present in the mesenchyme. Our data suggest that the axolotl has lost competency to activate strong canonical Wnt signaling in the epidermis and diverted this competence to the mesenchyme. Interestingly, *Rspondin2*, a potentiator of Wnt signaling in the mouse epidermis is expressed strictly in the mesenchyme in axolotl.

Pharmacological activation and inhibition of the Wnt pathway yielded results consistent with a role of Wnt signaling in promoting mesenchymal Amex.*Fgf8* expression. A positive effect of CHIR treatment on Amex.*Fgf8* expression was present after 3h of treatment but disappeared when the perturbation was performed for longer durations, possibly due to indirect effects or negative feedbacks triggered by the ubiquitously high Wnt signaling environment. The positive upstream regulatory role of Wnt signaling is similar to that seen in chicken and mammals yet occurring in a different tissue compartment (Barrow, Thomas et al. 2003, Soshnikova, Zechner et al. 2003). Our experiments have been performed at stages of limb development and regeneration subsequent to the initiation of Amex.*Fgf8* expression and therefore indicate a function of canonical Wnt signaling at least in maintaining Amex.*Fgf8* expression. In mouse and chick, canonical Wnt signaling is required for both the initiation and maintenance of endogenous Fgf8 expression and, when activated ectopically, can induce ectopic epidermal Fgf8 expression (Kengaku, Capdevila et al. 1998, Galceran, Farinas et al. 1999, Barrow, Thomas et al. 2003, Soshnikova, Zechner et al. 2003, Kawakami, Esteban et al. 2004). Interestingly, in the axolotl, canonical Wnt activation was not sufficient to induce ectopic Amex.*Fgf8* expression in the ectoderm. This difference may depend on a regulative process that is species-specific or on the method of experimental perturbation. Classical mouse and chick studies have not fully clarified if the Wnt-dependent induction of ectopic *Fgf8* expression is a direct and cell autonomous phenomenon. Ectopic *Fgf8*-expressing cells were often generated in stripes, suggesting that Wnt signaling may act to induce a local tissue re-organization that is likely dependent on additional signaling components, leaving open the possibility that ß-catenin pathway activation may not be sufficient to induce *Fgf8* expression cell autonomously in the mammalian and avian limb (Kengaku, Capdevila et al. 1998, Barrow, Thomas et al. 2003, Soshnikova, Zechner et al. 2003). Of the transcription factors that have been implicated in the regulation of AER *Fgf8* expression, Amex.*Lef1*, Amex.*Dlx5* and Amex.*Dlx6* were expressed also in the axolotl mesenchyme, where they may play a role in inducing or sustaining Amex.*Fgf8* expression. Nevertheless, their broad expression pattern includes portions of the limb mesenchyme devoid of Amex.*Fgf8* transcripts, suggesting they are not sufficient to induce Amex.*Fgf8* expression outside of its native domain.

In our study we also report that Amex.*Fgf10* expression is present not only in the axolotl limb mesenchyme but also in a small cell population localized in the basal layer of the limb bud and blastema epidermis. This additional expression domain is to our knowledge unique to the axolotl; *Fgf10* is considered a mesenchymal specific ligand, and the mesenchymal to epidermal *Fgf10-Fgfr2b* signaling interaction is conserved in the development of different organs across species, likely including the axolotl limb (Itoh 2016) (and this study). We show that the additional Amex.*Fgf10*-expressing population in the axolotl limb is not derived from the blastema mesenchyme and does not express the mesenchymal marker Amex.*Prrx1*. Consequently, it would be of interest to assess the function of these cells and of Amex.*Fgf10* expression in this additional domain, as well as to determine their lineage origin. They could be of ectodermal origin or derive from a different mesodermal linage. Interestingly,

Masselink et al showed that mesodermal cells of somitic origin are present in the zebrafish pectoral fin AER and that ablation of this cell population expands the Dre.*Fgf8* expression domain in the fin ectoderm (Masselink, Cole et al. 2016). Loss of this somitic mesoderm-derived cell population in the tetrapod limb has been speculated to be necessary for temporal expansion of *Fgf8* AER expression and fin to limb transition (Thorogood 1992). It is possible that in axolotl, where Amex.*Fgf8* expression is not epidermal, a somitic population has been maintained in the epidermis and carries functions that could be important for regeneration.

Further studies of axolotl limb patterning will help refine our understanding of the unique mechanisms that salamanders evolved to make a limb. Some of the adaptations of the axolotl limb patterning system may be important to accommodate specific requirements of limb regeneration, while features that are conserved across species may represent necessary elements of limb development. Mesenchymal expression of Amex.*Fgf8* is of particular interest as it has been implicated in anterior-posterior patterning and intercalation capability in limb regeneration (Shimizu-Nishikawa, Takahashi et al. 2003, Makanae and Satoh 2018). Our study highlights that the known regulators of AER *Fgf8* expression are present in the axolotl epidermis, where they are not sufficient to induce Amex.*Fgf8* expression and suggests that an epidermal to mesenchymal trade in sensitivity to canonical Wnt signaling may be an important factor for mesenchymal expression of Amex.*Fgf8* and a unique feature of limb development and regeneration in the axolotl or salamanders in general.

Materials & Methods

Axolotl Husbandry

d/d Axolotls were maintained in individual aquaria and all animal matings were undertaken in the IMP animal facility. All axolotl handling and surgical procedures were performed in accordance with local ethics committee guidelines. Animal experiments were performed as approved by the Magistrate of Vienna (animal license number GZ: 9418/2017/12).

Sample Harvesting

Prior to amputation, axolotls were anesthetized in 0.03% benzocaine (Sigma) solution until they no longer responded to physical stimuli. For expression profiling axolotl limb buds were harvested at stage 45-46. For expression profiling of blastema samples, forelimbs of axolotl snout-to-tail 3-4cm were amputated through the middle of the zeugopods and allowed to regenerate for 7 days before harvesting. Samples were fixed in 4% PFA at 4ºC overnight (14-17 hours) and then dehydrated progressively in a series of Methanol-PBS: 25-75%, 50-50%, 75-25% and 100% Methanol, each step on ice for at least 30 minutes. Samples were stored until usage at -20ºC in 100% Methanol. Prior to staining, limbs were rehydrated in progressively in 25-75%, 50-50%, 75-25% and 100-0% PBS-Methanol.

Drug treatments

Axolotls 3 to 4 cm from snout-to-tail were amputated as described above. Drug treatments were performed for different durations always starting at 5 days post amputation.
For the **12h IWR treatment,** 4 axolotls were treated for 12 hours with 25µM IWR-1-endo (Sigma, dissolved in DMSO), in a 30mL water bath, and 4 axolotls with the corresponding amount of DMSO as a control. All samples from this experiment were stained and imaged together on the same day.
For the **12h CHIR treatment,** 4 axolotls were treated for 12 hours with 50µM CHIR-99021 (Sigma, dissolved in DMSO), in a 30mL water bath, and 4 axolotls with the corresponding

amount of DMSO as a control. All samples from this experiment were stained and imaged together on the same day.
For the **3 and 6h CHIR treatment**, 6 axolotls were treated with 50µM CHIR or a DMSO control for either 3 or 6 hours, in a 15mL water bath. Limbs were stained and imaged in two rounds.

Whole-mount HCR *in situ* hybridization and tissue clearing
HCR probe pairs were designed against unique mRNA sequences common to all isoforms of the candidate gene, with the exception of Amex.*Fgfr2b* for which isoform specific probes were designed. Unique transcript sequences were identified by BLAST alignment of the sequence against the axolotl transcriptome Amex.T_v47 (Schloissnig, Kawaguchi et al. 2021) and eliminating transcript regions with a homology to non-target gene transcripts larger than 36 out of 50 nucleotides. Probes for Amex.*Fgf8,* Amex.*Fgf10,* Amex.*Fgfr2b* and Amex.*Prrx1*, hybridization wash and amplification buffers, as well as HCR hairpins were purchased from Molecular Instruments. The remaining probes were ordered as IDT Opools. For signal amplification, exclusively Alexa-546 and Alexa-647 conjugated hairpins were used in this study.

Limbs were stained using the whole-mount HCR protocol from Choi et al., 2018 with the following modifications. DAPI (Sigma, #D9542) was added with the hairpins at the amplification step. After washing in 5x SCCT, samples were washed for 2x 30’ in PBS and then cleared overnight incubating at room temperature in Ce3D solution. The Ce3D clearing media was prepared according to published methods (Li, Germain et al. 2017, Li, Germain et al. 2019), but without the use of 1-Thioglycerol (Anderson, Magidson et al. 2020). Whole-mount imaging was performed using a Z1 lightsheet microscope equipped with a 20x clearing objective (20x/1.53: Clr Plan-Neofluar 20x/1.0 Corr DIC; nd=1.53 WD= 6.4mm). The objective was set to match the RI of the clearing media (1.501) prior to imaging. HCR signal was excited using the 647nm and 561nm excitation wavelength lasers, while 488nm illumination was used to detect autofluorescence. DAPI was illuminated with the 405nm laser.

Section HCR Staining
After fixation, dehydration and rehydration, limbs were incubated overnight at 4ºC in 30% sucrose/PBS, transferred to OCT compound (Science Service), frozen on dry ice, and sectioned using a cryostat to a thickness of 12µm. HCR staining was performed according to the Choi et al., 2018 protocol for samples on a section. Sections were mounted using Abberior liquid antifade mounting media (#MM-2009-2X15ML). Slides were imaged with a Zeiss LSM 800 microscope with a 20x objective using the fast Airyscan detection mode. Raw images were Airyscan processed and stitched using Zen software.

Quantification of Whole-Mount Data
All image analysis was performed in Fiji (Schindelin, Arganda-Carreras et al. 2012). First, images were rotated and cropped in 3D using CLIJ2 (Haase, Royer et al. 2020), distal to the ulna and radius to exclude the mature stump and isolate the blastema. Subsequently background levels were calculated for each HCR channel by averaging multiple measurements of a 5µm x 5µm region of the epidermis devoid of any HCR signal and subtracted for each HCR channel.

Axolotl limb buds and blastemas contain blood cells that are highly auto fluorescent and can compromise the accuracy of signal quantifications. To address this issue, we acquired an

image of the autofluorescence in an empty channel (488nm illumination). We then segmented the gene expression domains, as well as the auto-fluorescent signal and subtracted auto-fluorescent regions from the gene expression domains.

To segment gene expression domains or auto-fluorescent structures, we first denoised the data using a 3D Gaussian blur (CLIJ2) with a sigma of x=6.0, y=6.0, z=1.74 pixels, corresponding to 3.84µm in all directions. We then thresholded manually the resulting image, isolating the expression domains in the 647nm- and 546nm-channel or auto-fluorescent structures in the 488nm-channel. Different thresholds were used for each channel, experiment, and imaging session, to account for fluctuations in laser power or staining efficacy but the same threshold was applied to all samples of the same experiment. The resulting segmentation masks were applied to the cropped raw data, after background subtraction, for 3D average intensity measurement using the 3D Roi Manager in Fiji (Ollion, Cochennec et al. 2013).

To measure *Axin2* expression in the epidermis, the mask of Amex.*Fgf8* expression domain was subtracted from the *Axin2* mask to isolate the epidermal Amex.*Axin2* expression domain (a low threshold for the Amex.*Fgf8* segmentation allows isolation of the entire mesenchymal domain, Supp. Fig. 8). The mesenchymal Amex.*Axin2* expression domain was further isolated by subtracting the epidermal mask from the Amex.*Axin2* mask.

The procedure was executed in automatic batch mode using Fiji macro scripting, statistical analysis and plotting were done using R software and the ggplot2 library (Wickham 2016, RStudio Team 2020, R Core Development Team 2021).

Statistical analysis

For the evaluation of the effect of pharmacological Wnt signaling perturbation on Amex.*Axin2* and Amex.*Fgf8* expression, the mean HCR intensity fluorescence in the segmented gene expression domains for a single blastema was used as a data point. Samples were grouped according to the treatment condition, and intensity data for each data point was normalized to the average of the DMSO control samples for the corresponding staining and treatment condition. Statistical comparison between sample groups and the corresponding DMSO controls was performed using the non-parametric Wilcoxon rank sum test.

For the 3h and 6h CHIR treatment, limbs were stained and imaged in two rounds. Data was normalized only to the DMSO samples imaged on the same day. After normalization, the data from the two different staining resulted not statistically different (Wilcoxon rank sum) and were therefore combined.

For all experiments, the number of replicates was decided empirically, and no samples were excluded. For the 12 hours CHIR treatment, there are 8 data points for Amex.*Fgf8* and 4 for Amex.*Axin2*, because 4 of the Amex.*Fgf8* stained samples were co-stained with a different marker.

Analogous statistical analysis was performed to compare Amex.*Axin2* HCR signal intensities in epidermis and mesenchyme (Fig. 5E).

Prrx1:Cre Lineage Tracing

Prrx1:Cre-ER;CAGGs:lp-Cherry axolotls were generated and tamoxifen converted during limb bud stages as described previously, to irreversibly label Prrx1 lineage mesenchymal

cells (Gerber, Murawala et al. 2018). Samples were processed for sectioning, staining and imaging as described above.

Single Cell Analysis
Single cell data was reanalyzed to match the latest axolotl transcriptome annotation (Schloissnig, Kawaguchi et al. 2021). The data was then was then imported into RStudio as a Seurat object, a data class specifically designed for manipulating scRNA seq data (Hao, Hao et al. 2021). Dimensionality reduction was performed using the FindClusters() function, with a resolution of 0.05—the resolution determines how many clusters will be generated from the data. To identify which clusters represent mesenchyme and epidermis, we plotted several marker genes of mesenchyme (Amex.*Prrx1*, Amex.*Fgf10*) and epidermis (Amex.*Krt12*, Amex.*Col17a1*, Amex.*Frem2*, Amex.*Epcam*) using the FeaturePlot() function. For Fig. 1 and 3, clusters were renamed 'mesenchyme' or 'epidermis' if they expressed corresponding marker genes, and all other clusters were made nameless. Markers for the other clusters are shown in Supp. Fig. 1 and 2. All subsequent plots were done using the FeaturePlot() function.

Figure compilation
All images were processed in Fiji and adjusted in brightness and contrast only for clarity (without gamma adjusting). Figure data plots were generated using R software. Figures were assembled in Adobe Illustrator.

Acknowledgments
We thank Francisco Falcon for re-analyzing the single cell datasets. We wish to thank Pavel Pasierbek and Alberto Moreno Cencerrado at the IMP Biooptics for their support. We thank Akane Kawaguchi and Leo Otsuki for advice and Magdalena Blaschek, Emina Silic, Tamara Torrecilla Lobos and Viktoria Szilagyi for axolotl care. We thank Osvaldo Chara and András Aszodi for statistical advice.
This work was supported by a Marshall Plan Foundation scholarship to GLG, and ERC AdG 7420346 and FWF I4846 grants to EMT.

References
Anderson, M. J., V. Magidson, R. Kageyama and M. Lewandoski (2020). "Fgf4 maintains Hes7 levels critical for normal somite segmentation clock function." Elife **9**.
Aoki, M., H. Kiyonari, H. Nakamura and H. Okamoto (2008). "R-spondin2 expression in the apical ectodermal ridge is essential for outgrowth and patterning in mouse limb development." Dev Growth Differ **50**(2): 85-95.
Barrow, J. R., K. R. Thomas, O. Boussadia-Zahui, R. Moore, R. Kemler, M. R. Capecchi and A. P. McMahon (2003). "Ectodermal Wnt3/beta-catenin signaling is required for the establishment and maintenance of the apical ectodermal ridge." Genes Dev **17**(3): 394-409.
Bell, S. M., C. M. Schreiner, S. E. Wert, M. L. Mucenski, W. J. Scott and J. A. Whitsett (2008). "R-spondin 2 is required for normal laryngeal-tracheal, lung and limb morphogenesis." Development **135**(6): 1049-1058.
Campbell, L. J. and C. M. Crews (2008). "Wound epidermis formation and function in urodele amphibian limb regeneration." Cell Mol Life Sci **65**(1): 73-79.
Carlson, B. M. (1975). "The effects of rotation and positional change of stump tissues upon morphogenesis of the regenerating axolotl limb." Dev Biol **47**(2): 269-291.
Choi, H. M. T., M. Schwarzkopf, M. E. Fornace, A. Acharya, G. Artavanis, J. Stegmaier, A. Cunha and N. A. Pierce (2018). "Third-generation in situ hybridization chain reaction: multiplexed, quantitative, sensitive, versatile, robust." Development **145**(12).

Christensen, R. N. and R. A. Tassava (2000). "Apical epithelial cap morphology and fibronectin gene expression in regenerating axolotl limbs." Dev Dyn **217**(2): 216-224.
Christensen, R. N., M. Weinstein and R. A. Tassava (2002). "Expression of fibroblast growth factors 4, 8, and 10 in limbs, flanks, and blastemas of Ambystoma." Dev Dyn **223**(2): 193-203.
De Moerlooze, L., B. Spencer-Dene, J. M. Revest, M. Hajihosseini, I. Rosewell and C. Dickson (2000). "An important role for the IIIb isoform of fibroblast growth factor receptor 2 (FGFR2) in mesenchymal-epithelial signalling during mouse organogenesis." Development **127**(3): 483-492.
Eckei, G., M. Boing, B. Brand-Saberi and G. Morosan-Puopolo (2016). "Expression Pattern of Axin2 During Chicken Development." PLoS One **11**(9): e0163610.
Frobisch, N. B., C. Bickelmann, J. C. Olori and F. Witzmann (2015). "Deep-time evolution of regeneration and preaxial polarity in tetrapod limb development." Nature **527**(7577): 231-234.
Galceran, J., I. Farinas, M. J. Depew, H. Clevers and R. Grosschedl (1999). "Wnt3a-/--like phenotype and limb deficiency in Lef1(-/-)Tcf1(-/-) mice." Genes Dev **13**(6): 709-717.
Gerber, T., P. Murawala, D. Knapp, W. Masselink, M. Schuez, S. Hermann, M. Gac-Santel, S. Nowoshilow, J. Kageyama, S. Khattak, J. D. Currie, J. G. Camp, E. M. Tanaka and B. Treutlein (2018). "Single-cell analysis uncovers convergence of cell identities during axolotl limb regeneration." Science **362**(6413).
Haase, R., L. A. Royer, P. Steinbach, D. Schmidt, A. Dibrov, U. Schmidt, M. Weigert, N. Maghelli, P. Tomancak, F. Jug and E. W. Myers (2020). "CLIJ: GPU-accelerated image processing for everyone." Nat Methods **17**(1): 5-6.
Hao, Y., S. Hao, E. Andersen-Nissen, W. M. Mauck, 3rd, S. Zheng, A. Butler, M. J. Lee, A. J. Wilk, C. Darby, M. Zager, P. Hoffman, M. Stoeckius, E. Papalexi, E. P. Mimitou, J. Jain, A. Srivastava, T. Stuart, L. M. Fleming, B. Yeung, A. J. Rogers, J. M. McElrath, C. A. Blish, R. Gottardo, P. Smibert and R. Satija (2021). "Integrated analysis of multimodal single-cell data." Cell **184**(13): 3573-3587 e3529.
Haro, E., I. Delgado, M. Junco, Y. Yamada, A. Mansouri, K. C. Oberg and M. A. Ros (2014). "Sp6 and Sp8 transcription factors control AER formation and dorsal-ventral patterning in limb development." PLoS Genet **10**(8): e1004468.
Hill, T. P., M. M. Taketo, W. Birchmeier and C. Hartmann (2006). "Multiple roles of mesenchymal beta-catenin during murine limb patterning." Development **133**(7): 1219-1229.
Itoh, N. (2016). "FGF10: A multifunctional mesenchymal-epithelial signaling growth factor in development, health, and disease." Cytokine Growth Factor Rev **28**: 63-69.
Itou, J., N. Taniguchi, I. Oishi, H. Kawakami, M. Lotz and Y. Kawakami (2011). "HMGB factors are required for posterior digit development through integrating signaling pathway activities." Dev Dyn **240**(5): 1151-1162.
Kawakami, Y., J. Capdevila, D. Buscher, T. Itoh, C. Rodriguez Esteban and J. C. Izpisua Belmonte (2001). "WNT signals control FGF-dependent limb initiation and AER induction in the chick embryo." Cell **104**(6): 891-900.
Kawakami, Y., C. R. Esteban, T. Matsui, J. Rodriguez-Leon, S. Kato and J. C. Izpisua Belmonte (2004). "Sp8 and Sp9, two closely related buttonhead-like transcription factors, regulate Fgf8 expression and limb outgrowth in vertebrate embryos." Development **131**(19): 4763-4774.
Kawakami, Y., C. Rodriguez Esteban, M. Raya, H. Kawakami, M. Marti, I. Dubova and J. C. Izpisua Belmonte (2006). "Wnt/beta-catenin signaling regulates vertebrate limb regeneration." Genes Dev **20**(23): 3232-3237.

Kengaku, M., J. Capdevila, C. Rodriguez-Esteban, J. De La Pena, R. L. Johnson, J. C. Izpisua Belmonte and C. J. Tabin (1998). "Distinct WNT pathways regulating AER formation and dorsoventral polarity in the chick limb bud." Science **280**(5367): 1274-1277.
Knapp, D., H. Schulz, C. A. Rascon, M. Volkmer, J. Scholz, E. Nacu, M. Le, S. Novozhilov, A. Tazaki, S. Protze, T. Jacob, N. Hubner, B. Habermann and E. M. Tanaka (2013). "Comparative transcriptional profiling of the axolotl limb identifies a tripartite regeneration-specific gene program." PLoS One **8**(5): e61352.
Laufer, E., C. E. Nelson, R. L. Johnson, B. A. Morgan and C. Tabin (1994). "Sonic hedgehog and Fgf-4 act through a signaling cascade and feedback loop to integrate growth and patterning of the developing limb bud." Cell **79**(6): 993-1003.
Leigh, N. D., G. S. Dunlap, K. Johnson, R. Mariano, R. Oshiro, A. Y. Wong, D. M. Bryant, B. M. Miller, A. Ratner, A. Chen, W. W. Ye, B. J. Haas and J. L. Whited (2018). "Transcriptomic landscape of the blastema niche in regenerating adult axolotl limbs at single-cell resolution." Nat Commun **9**(1): 5153.
Lewandoski, M., X. Sun and G. R. Martin (2000). "Fgf8 signalling from the AER is essential for normal limb development." Nat Genet **26**(4): 460-463.
Li, H., X. Wei, L. Zhou, W. Zhang, C. Wang, Y. Guo, D. Li, J. Chen, T. Liu, Y. Zhang, S. Ma, C. Wang, F. Tan, J. Xu, Y. Liu, Y. Yuan, L. Chen, Q. Wang, J. Qu, Y. Shen, S. Liu, G. Fan, L. Liu, X. Liu, Y. Hou, G. H. Liu, Y. Gu and X. Xu (2021). "Dynamic cell transition and immune response landscapes of axolotl limb regeneration revealed by single-cell analysis." Protein Cell **12**(1): 57-66.
Li, W., R. N. Germain and M. Y. Gerner (2017). "Multiplex, quantitative cellular analysis in large tissue volumes with clearing-enhanced 3D microscopy (Ce3D)." Proc Natl Acad Sci U S A **114**(35): E7321-E7330.
Li, W., R. N. Germain and M. Y. Gerner (2019). "High-dimensional cell-level analysis of tissues with Ce3D multiplex volume imaging." Nat Protoc **14**(6): 1708-1733.
Lin, C., Y. Yin, S. M. Bell, G. M. Veith, H. Chen, S. H. Huh, D. M. Ornitz and L. Ma (2013). "Delineating a conserved genetic cassette promoting outgrowth of body appendages." PLoS Genet **9**(1): e1003231.
Lin, T. Y., T. Gerber, Y. Taniguchi-Sugiura, P. Murawala, S. Hermann, L. Grosser, E. Shibata, B. Treutlein and E. M. Tanaka (2021). "Fibroblast dedifferentiation as a determinant of successful regeneration." Dev Cell **56**(10): 1541-1551 e1546.
Makanae, A. and A. Satoh (2018). "Ectopic Fgf signaling induces the intercalary response in developing chicken limb buds." Zoological Lett **4**: 8.
Mariani, F. V., C. P. Ahn and G. R. Martin (2008). "Genetic evidence that FGFs have an instructive role in limb proximal-distal patterning." Nature **453**(7193): 401-405.
Marinic, M., T. Aktas, S. Ruf and F. Spitz (2013). "An integrated holo-enhancer unit defines tissue and gene specificity of the Fgf8 regulatory landscape." Dev Cell **24**(5): 530-542.
Masselink, W., N. J. Cole, F. Fenyes, S. Berger, C. Sonntag, A. Wood, P. D. Nguyen, N. Cohen, F. Knopf, G. Weidinger, T. E. Hall and P. D. Currie (2016). "A somitic contribution to the apical ectodermal ridge is essential for fin formation." Nature **535**(7613): 542-546.
Moon, A. M. and M. R. Capecchi (2000). "Fgf8 is required for outgrowth and patterning of the limbs." Nat Genet **26**(4): 455-459.
Nacu, E., E. Gromberg, C. R. Oliveira, D. Drechsel and E. M. Tanaka (2016). "FGF8 and SHH substitute for anterior-posterior tissue interactions to induce limb regeneration." Nature **533**(7603): 407-410.
Nam, J. S., E. Park, T. J. Turcotte, S. Palencia, X. Zhan, J. Lee, K. Yun, W. D. Funk and J. K. Yoon (2007). "Mouse R-spondin2 is required for apical ectodermal ridge maintenance in the hindlimb." Dev Biol **311**(1): 124-135.

Niswander, L., S. Jeffrey, G. R. Martin and C. Tickle (1994). "A positive feedback loop coordinates growth and patterning in the vertebrate limb." Nature **371**(6498): 609-612.
Nusse, R. and H. Clevers (2017). "Wnt/beta-Catenin Signaling, Disease, and Emerging Therapeutic Modalities." Cell **169**(6): 985-999.
Nye, H. L., J. A. Cameron, E. A. Chernoff and D. L. Stocum (2003). "Extending the table of stages of normal development of the axolotl: limb development." Dev Dyn **226**(3): 555-560.
Ollion, J., J. Cochennec, F. Loll, C. Escude and T. Boudier (2013). "TANGO: a generic tool for high-throughput 3D image analysis for studying nuclear organization." Bioinformatics **29**(14): 1840-1841.
Poulin, M. L. and I. M. Chiu (1995). "Re-programming of expression of the KGFR and bek variants of fibroblast growth factor receptor 2 during limb regeneration in newts (Notophthalmus viridescens)." Dev Dyn **202**(4): 378-387.
Purushothaman, S., A. Elewa and A. W. Seifert (2021). "Correction: Fgf-signaling is compartmentalized within the mesenchyme and controls proliferation during salamander limb development." Elife **10**.
R Core Development Team (2021). R: A Language and Environment for Statistical Computing.
Robledo, R. F., L. Rajan, X. Li and T. Lufkin (2002). "The Dlx5 and Dlx6 homeobox genes are essential for craniofacial, axial, and appendicular skeletal development." Genes Dev **16**(9): 1089-1101.
Rodgers, A. K., J. J. Smith and S. R. Voss (2020). "Identification of immune and non-immune cells in regenerating axolotl limbs by single-cell sequencing." Exp Cell Res **394**(2): 112149.
RStudio Team (2020). "RStudio: Integrated Development Environment for R."
Schindelin, J., I. Arganda-Carreras, E. Frise, V. Kaynig, M. Longair, T. Pietzsch, S. Preibisch, C. Rueden, S. Saalfeld, B. Schmid, J. Y. Tinevez, D. J. White, V. Hartenstein, K. Eliceiri, P. Tomancak and A. Cardona (2012). "Fiji: an open-source platform for biological-image analysis." Nat Methods **9**(7): 676-682.
Schloissnig, S., A. Kawaguchi, S. Nowoshilow, F. Falcon, L. Otsuki, P. Tardivo, N. Timoshevskaya, M. C. Keinath, J. J. Smith, S. R. Voss and E. M. Tanaka (2021). "The giant axolotl genome uncovers the evolution, scaling, and transcriptional control of complex gene loci." Proc Natl Acad Sci U S A **118**(15).
Sekine, K., H. Ohuchi, M. Fujiwara, M. Yamasaki, T. Yoshizawa, T. Sato, N. Yagishita, D. Matsui, Y. Koga, N. Itoh and S. Kato (2019). "Fgf10 is essential for limb and lung formation (vol 21, pg 138, 1999)." Nature Genetics **51**(5): 921-921.
Shimizu-Nishikawa, K., J. Takahashi and A. Nishikawa (2003). "Intercalary and supernumerary regeneration in the limbs of the frog, Xenopus laevis." Dev Dyn **227**(4): 563-572.
Shubin NH, A. P. (1986). "A morphogenetic approach to the origin and basic organization of the tetrapod limb." Evolutionary Biology.
Singh, B. N., M. J. Doyle, C. V. Weaver, N. Koyano-Nakagawa and D. J. Garry (2012). "Hedgehog and Wnt coordinate signaling in myogenic progenitors and regulate limb regeneration." Dev Biol **371**(1): 23-34.
Soshnikova, N., D. Zechner, J. Huelsken, Y. Mishina, R. R. Behringer, M. M. Taketo, E. B. Crenshaw, 3rd and W. Birchmeier (2003). "Genetic interaction between Wnt/beta-catenin and BMP receptor signaling during formation of the AER and the dorsal-ventral axis in the limb." Genes Dev **17**(16): 1963-1968.
Sugiura, T., H. Wang, R. Barsacchi, A. Simon and E. M. Tanaka (2016). "MARCKS-like protein is an initiating molecule in axolotl appendage regeneration." Nature **531**(7593): 237-240.

Sun, X., F. V. Mariani and G. R. Martin (2002). "Functions of FGF signalling from the apical ectodermal ridge in limb development." Nature **418**(6897): 501-508.
Szenker-Ravi, E., U. Altunoglu, M. Leushacke, C. Bosso-Lefevre, M. Khatoo, H. Thi Tran, T. Naert, R. Noelanders, A. Hajamohideen, C. Beneteau, S. B. de Sousa, B. Karaman, X. Latypova, S. Basaran, E. B. Yucel, T. T. Tan, L. Vlaminck, S. S. Nayak, A. Shukla, K. M. Girisha, C. Le Caignec, N. Soshnikova, Z. O. Uyguner, K. Vleminckx, N. Barker, H. Kayserili and B. Reversade (2018). "RSPO2 inhibition of RNF43 and ZNRF3 governs limb development independently of LGR4/5/6." Nature **557**(7706): 564-569.
Talamillo, A., I. Delgado, T. Nakamura, S. de-Vega, Y. Yoshitomi, F. Unda, W. Birchmeier, Y. Yamada and M. A. Ros (2010). "Role of Epiprofin, a zinc-finger transcription factor, in limb development." Dev Biol **337**(2): 363-374.
Thornton, C. S. (1957). "The effect of apical cap removal on limb regeneration in Amblystoma larvae." J Exp Zool **134**(2): 357-381.
Thorogood, P. (1992). "Developmental Patterning of the Vertebrate Limb - Hinchliffe,Jr, Hurle,Jm, Summerbell,D." Science **257**(5076): 1570-1571.
Wickham, H. (2016). ggplot2: Elegant Graphics for Data Analysis, Springer-Verlag New York.
Wischin, S., C. Castaneda-Patlan, M. Robles-Flores and J. Chimal-Monroy (2017). "Chemical activation of Wnt/beta-catenin signalling inhibits innervation and causes skeletal tissue malformations during axolotl limb regeneration." Mech Dev **144**(Pt B): 182-190.
Xu, X., M. Weinstein, C. Li, M. Naski, R. I. Cohen, D. M. Ornitz, P. Leder and C. Deng (1998). "Fibroblast growth factor receptor 2 (FGFR2)-mediated reciprocal regulation loop between FGF8 and FGF10 is essential for limb induction." Development **125**(4): 753-765.
Yamada, W., K. Nagao, K. Horikoshi, A. Fujikura, E. Ikeda, Y. Inagaki, M. Kakitani, K. Tomizuka, H. Miyazaki, T. Suda and K. Takubo (2009). "Craniofacial malformation in R-spondin2 knockout mice." Biochem Biophys Res Commun **381**(3): 453-458.
Zhang, X., O. A. Ibrahimi, S. K. Olsen, H. Umemori, M. Mohammadi and D. M. Ornitz (2006). "Receptor specificity of the fibroblast growth factor family. The complete mammalian FGF family." J Biol Chem **281**(23): 15694-15700.
Zuniga, A. and R. Zeller (2020). "Dynamic and self-regulatory interactions among gene regulatory networks control vertebrate limb bud morphogenesis." Curr Top Dev Biol **139**: 61-88.

Figure 1.

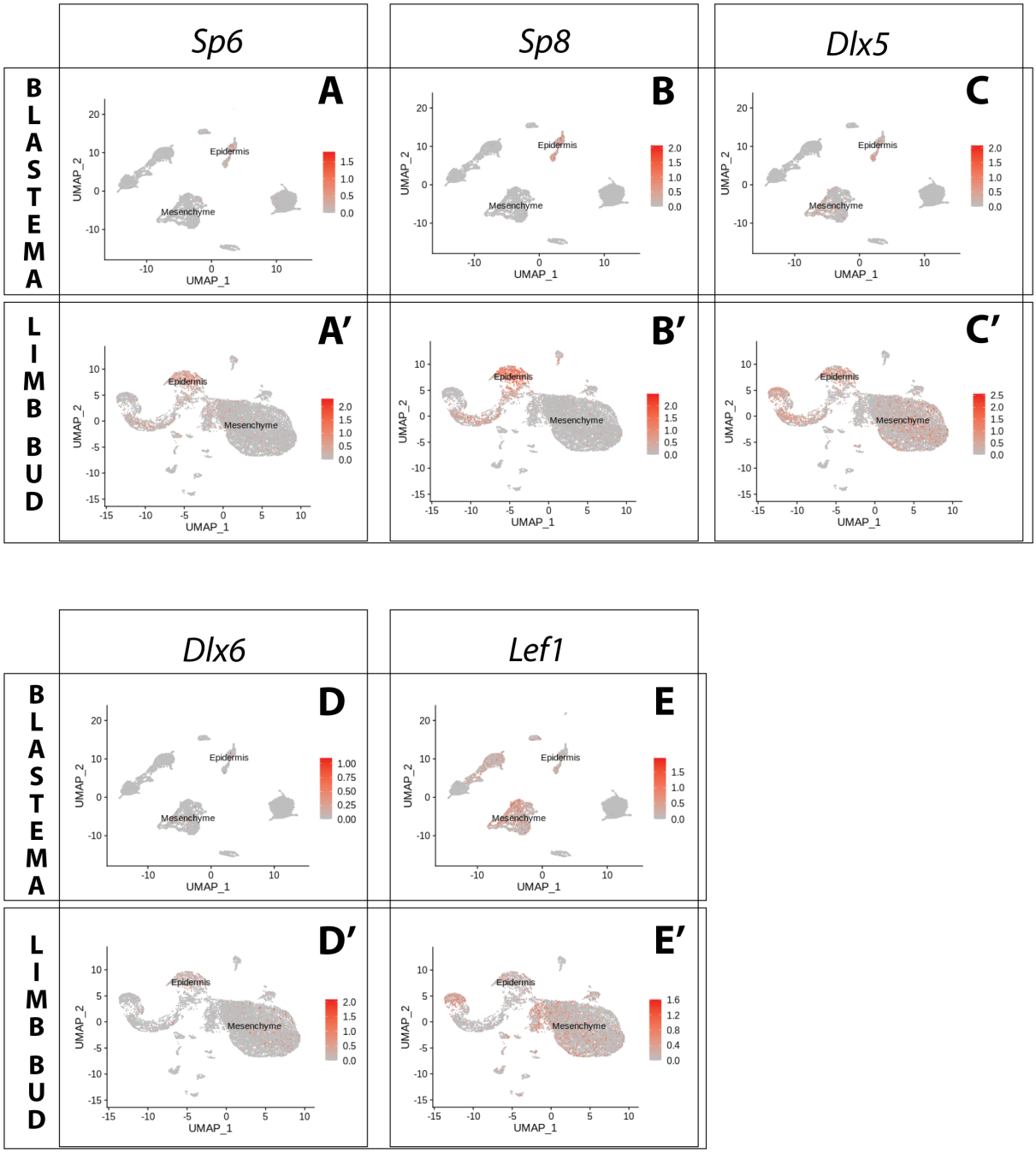

Figure 1. Expression of AER transcription factors in the axolotl limb bud and limb blastema assessed by re-analysis of Axolotl scRNA seq datasets.
Re-analysis of scRNA seq data from blastema (A,B,C,D,E, data from *Li, Wei et al. 2021*) or limb bud (A',B',C',D',E', data from *Lin, Gerber et al. 2021*).
A,A'. UMAPs of Axolotl scRNA seq expression data for *Sp6.* Expression is detected in the epidermis of the axolotl blastema and limb bud.
B,B'. UMAPs of Axolotl scRNA seq expression data for *Sp8.* Expression is detected in the epidermis of the axolotl blastema and limb bud.
C,C'. UMAPs of Axolotl scRNA seq expression data for *Dlx5.* Expression is detected in the epidermis and mesenchyme of the axolotl blastema and limb bud.

D,D'. UMAPs of Axolotl scRNA seq expression data for *Dlx6.* Expression is detected in the epidermis and mesenchyme of the axolotl limb bud. Expression is detected only in few blastema cells.
E,E'. UMAPs of Axolotl scRNA seq expression data for *Lef1.* Expression is detected in the epidermis and mesenchyme of the axolotl blastema and limb bud.

Figure 2.

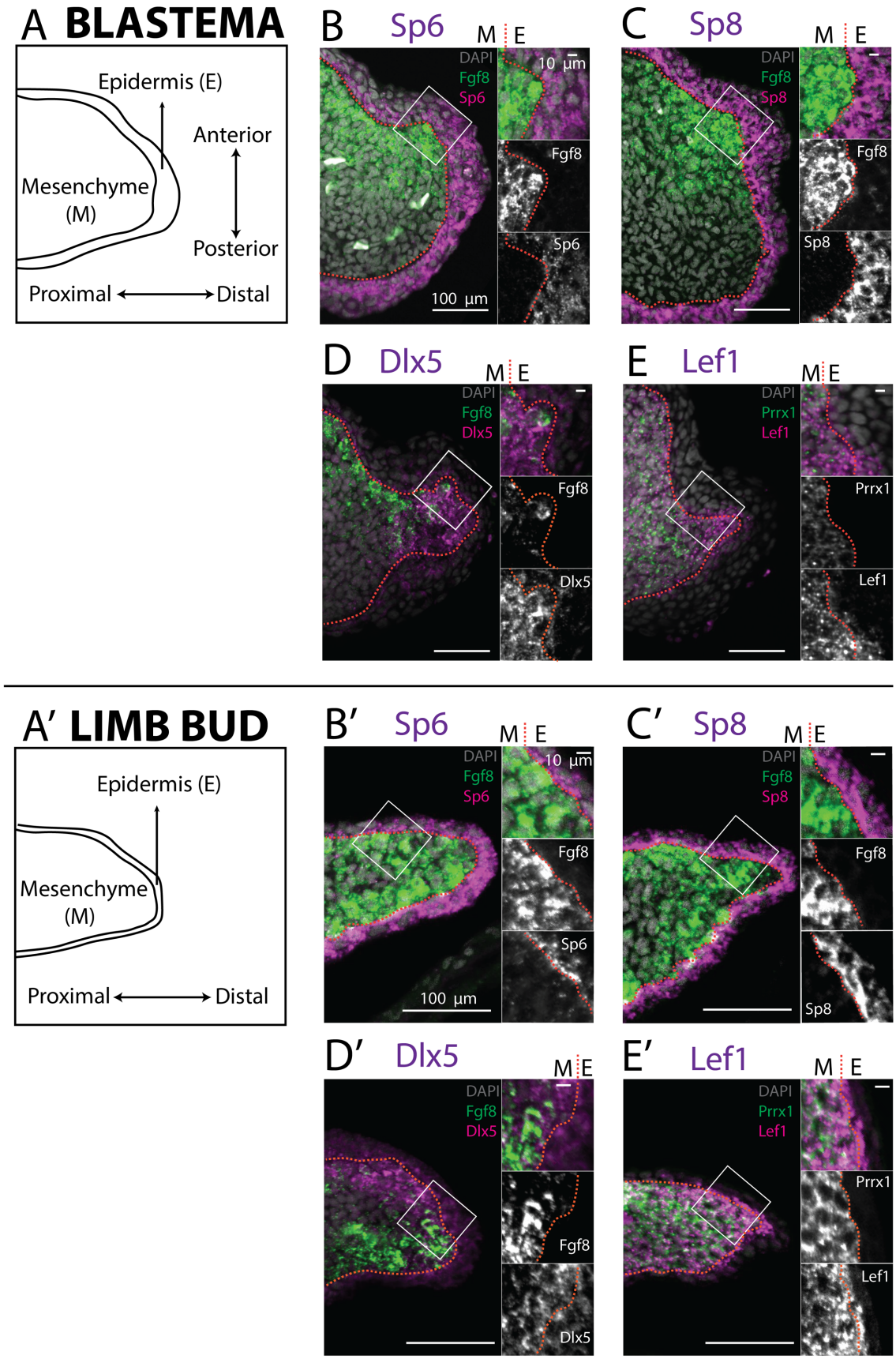
A BLASTEMA
Epidermis (E)
Anterior
Mesenchyme (M)
Posterior
Proximal
Distal
B Sp6
M E
DAPI
Fgf8
Sp6
10 µm
100 µm
C Sp8
Sp8
D Dlx5
Dlx5
E Lef1
Prrx1
Lef1
A′ LIMB BUD
B′ Sp6
C′ Sp8
D′ Dlx5
E′ Lef1

Figure 2. Expression of AER transcription factors in the axolotl limb blastema and limb bud assessed by HCR *in situ* hybridization.
A, A'. Schematic outlining the mesenchymal and epidermal compartments in a longitudinal section of an axolotl blastema and limb bud.
B, B'. Expression of *Sp6* in the epidermis and of *Fgf8* in the mesenchyme of the axolotl blastema and limb bud revealed by HCR (single planes from whole mount images, n=4).
C, C'. Expression of *Sp8* in the epidermis and of *Fgf8* in the mesenchyme of the axolotl blastema and limb bud revealed by HCR (single planes from whole mount images, n=4).
D, D'. Expression of *Fgf8* in the mesenchyme as well as of *Dlx5* in the mesenchyme and basal epidermis of the axolotl limb bud and blastema (single planes from whole mount images, n=4).
E, E'. Expression of the mesenchymal marker *Prrx1,* and of *Lef1* in the mesenchyme and basal epidermis of the axolotl blastema and limb bud (single planes from whole mount images, n=4)
For microscopy images right panels represent magnifications of the outlined boxes, M = mesenchyme, E = epidermis. Dashed lines demarcate epidermal-mesenchymal boundaries.

Figure 3.

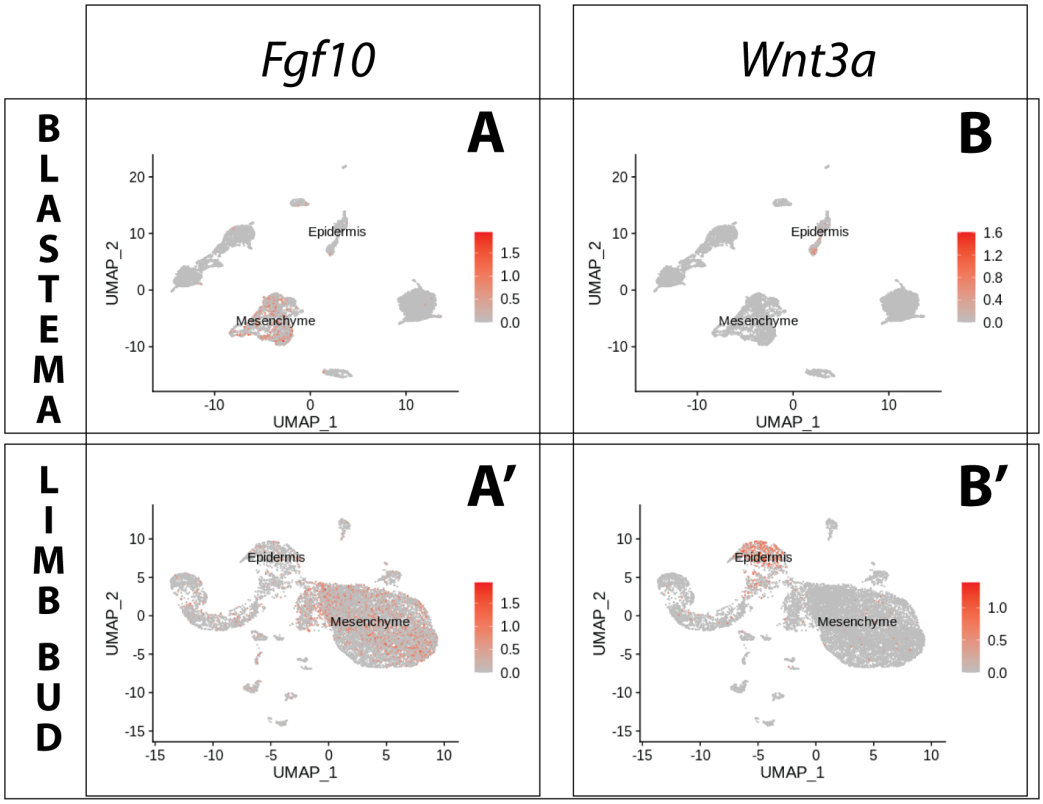
Fgf10
Wnt3a
BLASTEMA
LIMB BUD
A
B
A'
B'
Epidermis
Mesenchyme
UMAP_1
UMAP_2

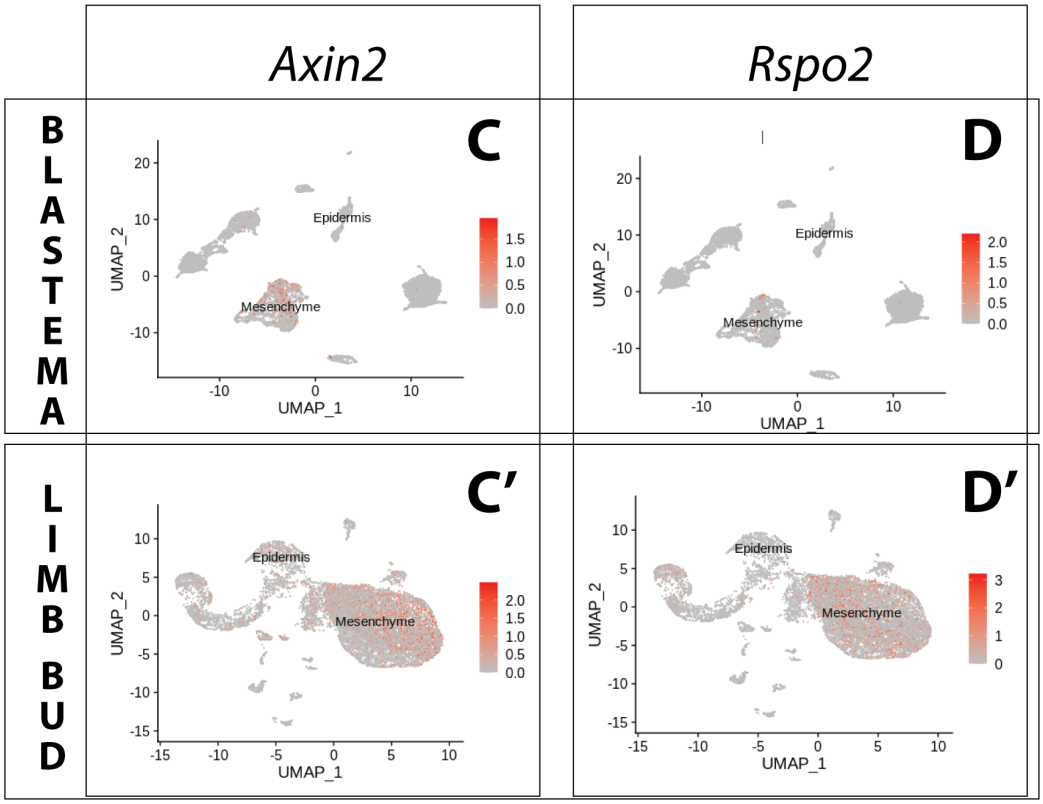
Axin2
Rspo2
BLASTEMA
LIMB BUD
C
D
C'
D'
Epidermis
Mesenchyme
UMAP_1
UMAP_2

Figure 3. Expression of *Fgf10* and of the canonical Wnt pathway components *Wnt3a, Axin2, Rspo2* in the axolotl limb bud and limb blastema assessed by re-analysis of Axolotl scRNA seq datasets.
Re-analysis of scRNA seq data from blastema (A,B,C,D, data from *Li, Wei et al. 2021*) or limb bud (A',B',C',D', data from *Lin, Gerber et al. 2021*).
A,A'. UMAPs of Axolotl scRNA seq expression data for *Fgf10.* Expression is detected in the mesenchyme of the axolotl blastema and limb bud.
B,B'. UMAPs of Axolotl scRNA seq expression data for *Wnt3a.* Expression is detected in the epidermis of the axolotl blastema and limb bud.
C,C'. UMAPs of Axolotl scRNA seq expression data for *Axin2.* Expression is detected in the prevalently in the mesenchyme of the axolotl blastema and limb bud.
D,D'. UMAPs of Axolotl scRNA seq expression data for *Rspo2.* Expression is detected in the mesenchyme of the axolotl limb bud. Expression is detected only in few blastema cells.

Figure 4

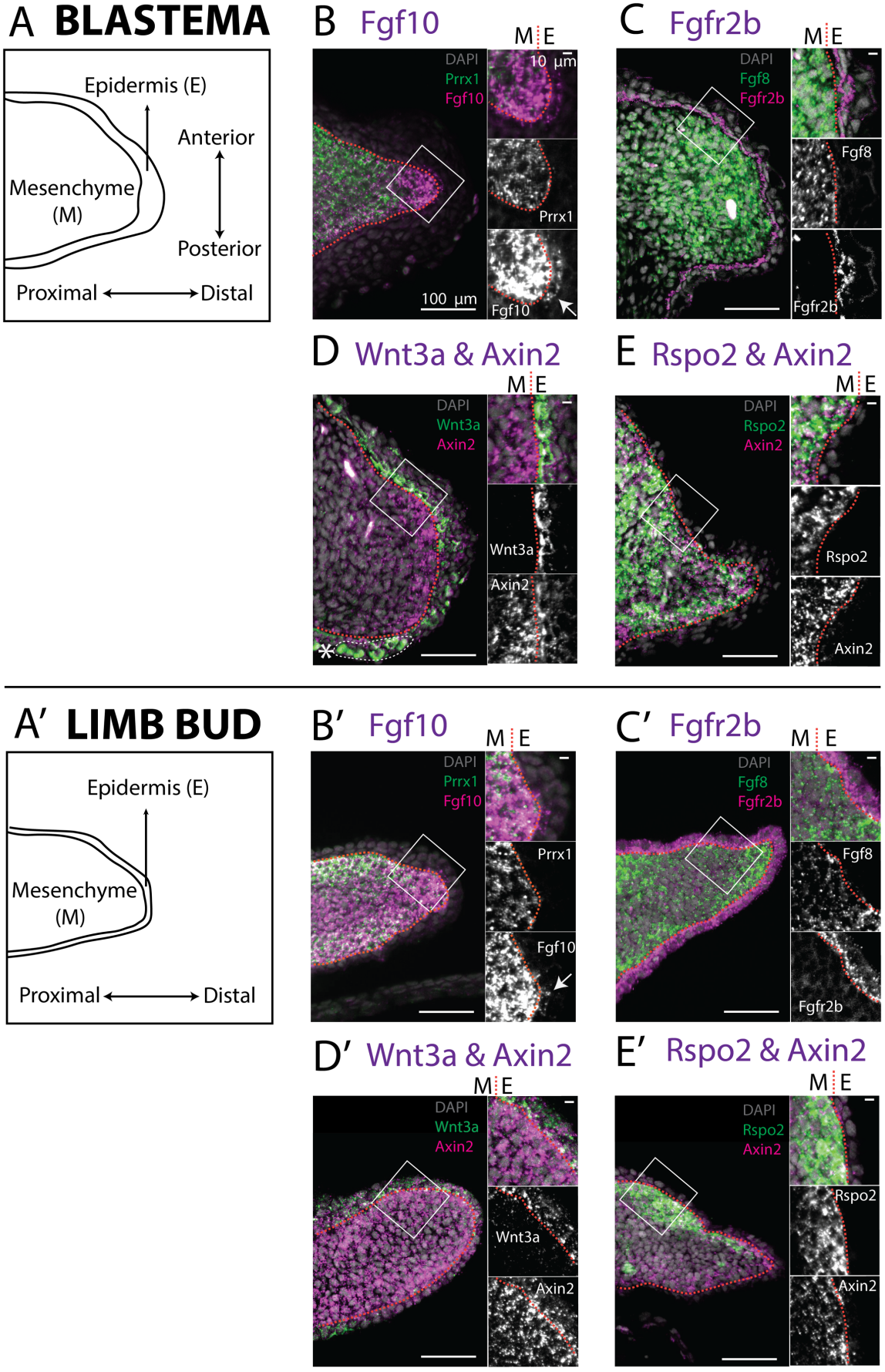
A BLASTEMA
Epidermis (E)
Anterior
Mesenchyme (M)
Posterior
Proximal
Distal
B Fgf10
M E
DAPI
Prrx1
Fgf10
10 µm
100 µm
C Fgfr2b
DAPI
Fgf8
Fgfr2b
D Wnt3a & Axin2
Wnt3a
Axin2
E Rspo2 & Axin2
Rspo2
A′ LIMB BUD
B′ Fgf10
C′ Fgfr2b
D′ Wnt3a & Axin2
E′ Rspo2 & Axin2

Figure 4. Expression of *Fgf10, Fgfr2b* and of the canonical Wnt pathway components *Wnt3a, Axin2, Rspo2* in the axolotl limb bud and limb blastema evaluated by HCR in situ hybridization.

A, A'. Schematic outlining the mesenchymal and epidermal compartments in a longitudinal section of an axolotl blastema and limb bud.

B,B'. Expression of *Prrx1* and *Fgf10* in the mesenchyme of the axolotl blastema and limb bud revealed by HCR (single planes from whole mount images, n=4). Arrows point to weak *Fgf10* expression present in the distal basal epidermis of the blastema and limb bud.

C,C'. Expression of *Fgf8* in the mesenchyme and expression of *Fgfr2b* in the basal epidermis of the axolotl blastema and limb bud revealed by HCR (single planes from whole mount images, n=4).

D,D'. Expression of *Wnt3a* in the basal epidermis and *Axin2* in the mesenchyme and basal epidermis of the axolotl blastema and limb bud (single planes from whole mount images, n=4). *Axin2* expression is stronger in the mesenchyme and weaker in the epidermis.

E,E'. Expression of *Rspo2* in the mesenchyme and *Axin2* in the mesenchyme and basal epidermis of the axolotl blastema and limb bud (single plane from whole mount image, n=4). Bright green structures (*) in the blastema outer epidermis are auto-fluorescent signal.

For microscopy images right panels represent magnifications of the outlined boxes, M = mesenchyme, E = epidermis. Dashed lines demarcate epidermal-mesenchymal boundaries.

Figure 5.

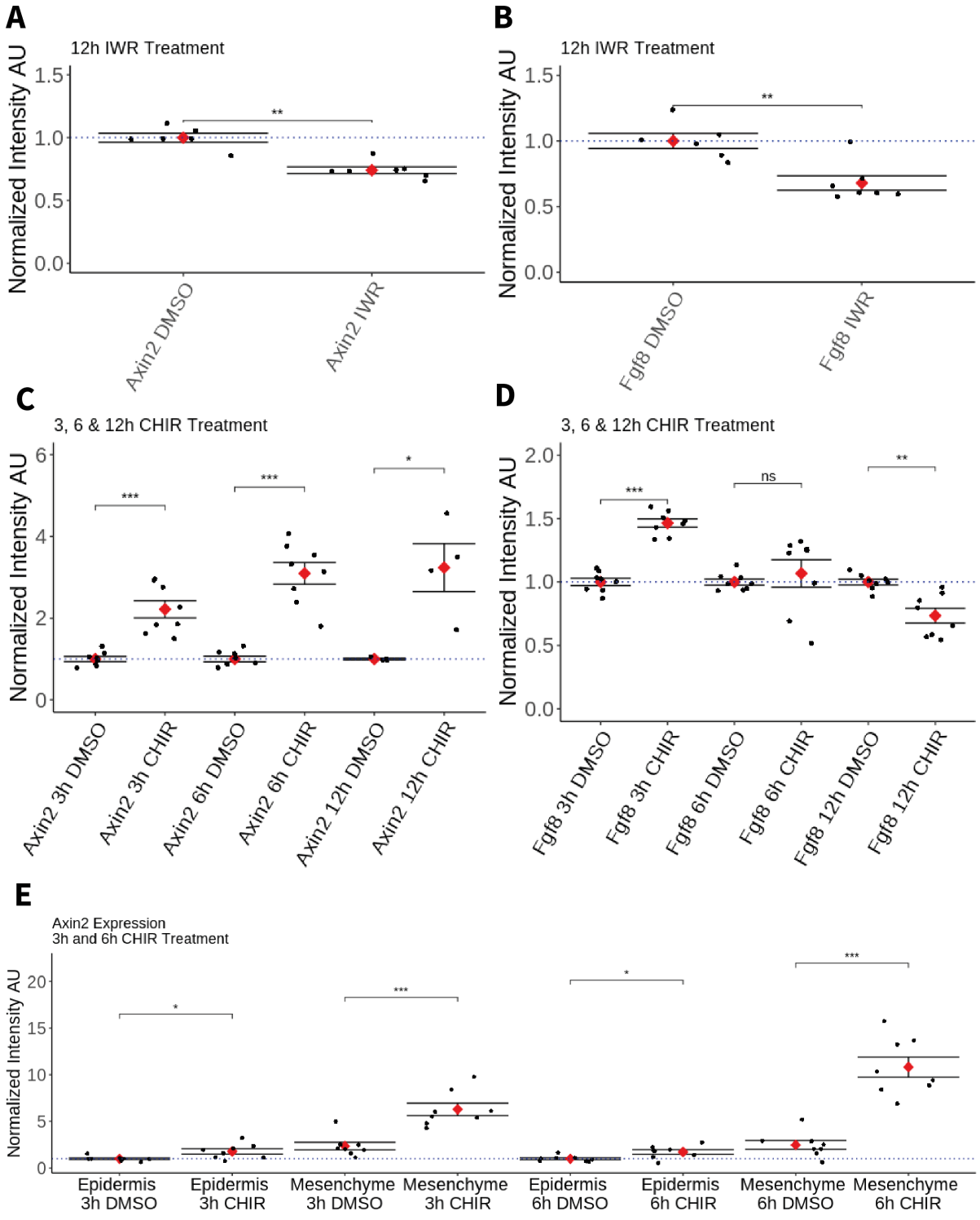
A
12h IWR Treatment
Normalized Intensity AU
1.5
1.0
0.5
0.0
**
Axin2 DMSO
Axin2 IWR
B
12h IWR Treatment
Normalized Intensity AU
1.5
1.0
0.5
0.0
**
Fgf8 DMSO
Fgf8 IWR
C
3, 6 & 12h CHIR Treatment
Normalized Intensity AU
6
4
2
0
***
***
*
Axin2 3h DMSO
Axin2 3h CHIR
Axin2 6h DMSO
Axin2 6h CHIR
Axin2 12h DMSO
Axin2 12h CHIR
D
3, 6 & 12h CHIR Treatment
Normalized Intensity AU
2.0
1.5
1.0
0.5
0.0
***
ns
**
Fgf8 3h DMSO
Fgf8 3h CHIR
Fgf8 6h DMSO
Fgf8 6h CHIR
Fgf8 12h DMSO
Fgf8 12h CHIR
E
Axin2 Expression
3h and 6h CHIR Treatment
Normalized Intensity AU
20
15
10
5
0
*
***
*
***
Epidermis 3h DMSO
Epidermis 3h CHIR
Mesenchyme 3h DMSO
Mesenchyme 3h CHIR
Epidermis 6h DMSO
Epidermis 6h CHIR
Mesenchyme 6h DMSO
Mesenchyme 6h CHIR

Figure 5. Effect of pharmacological perturbation of Wnt signaling on *Fgf8* expression in the axolotl blastema.

Plots depicting expression levels of *Fgf8* or *Axin2* as assessed by mean fluorescent intensity of HCR signal inside the corresponding gene expression domains. Each black dot represents the mean signal quantified from one blastema, each red dot represents mean values for each condition. Whiskers indicate the standard error of the mean. * indicates statistical significance (* $p<0.05$, ** $p<0.01$, *** $p<0.001$, ns= non-significant=p>05). Statistics were performed using the non-parametric Wilcoxon rank sum test.

A,B. Pharmacological inhibition of Wnt signaling using IWR1-endo downregulates *Axin2* and *Fgf8* expression in the axolotl limb blastema.

C. CHIR treatment activates canonical Wnt signaling in the axolotl blastema as shown by upregulation of *Axin2* expression after 3, 6 and 12 hours of treatment.

D. Pharmacological activation of Wnt signaling using CHIR upregulates *Fgf8* in the axolotl blastema after 3 hours of treatment. *Fgf8* expression comparable to DMSO control levels after 6 hours of treatment and downregulated after 12 hours of CHIR treatment.

E. Mesenchymal and epidermal *Axin2* expression are both upregulated after 3 and 6 hours of CHIR treatment. Mesenchymal *Axin2* increases 2.6-fold after 3 hours and 4.4-fold after 6 hours of treatment. Epidermal *Axin2* increases 1.8-fold after 3 hours and 1.7-fold after 6 hours of treatment.

Supplementary Figures.

Supplementary Figure 1.

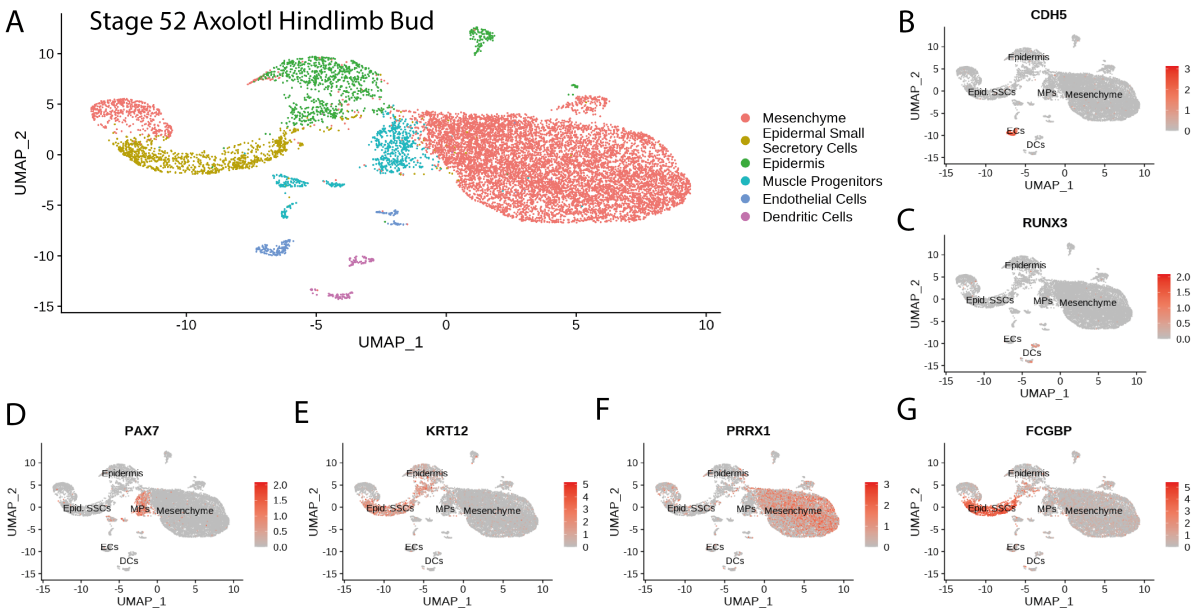

Supplementary Figure 1. Cluster identification in the re-analysis of axolotl limb bud scRNA seq dataset from *Lin, Gerber et al. 2021.*

A. Clustering of axolotl limb bud scRNA seq expression data reveals six clusters that are readily identifiable by the expression of key markers.

B. *Cdh5* labels endothelial cells in the axolotl limb bud scRNA seq dataset.

C. *Runx3* labels dendritic cells in the axolotl limb bud scRNA seq dataset.

D. *Pax7* labels muscle progenitors in the axolotl limb bud scRNA seq dataset.

E. *Krt12* labels epidermal cells (including SSCs) in the axolotl limb bud scRNA seq dataset.

F. *Prrx1* labels mesenchymal cells in the axolotl limb bud scRNA seq dataset.

G. *Fcgbp* labels epidermal small secretory cells in the axolotl limb bud scRNA seq dataset.

Supplementary Figure 2.

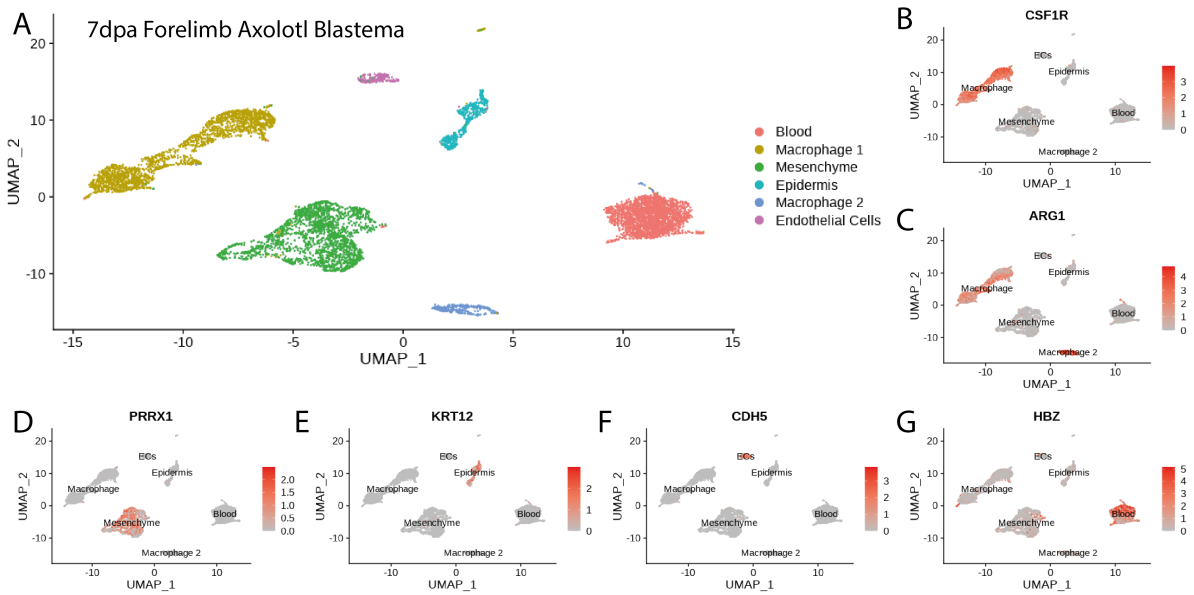

Supplementary Figure 2. Cluster identification in the re-analysis of axolotl blastema scRNA seq dataset from *Li, Wei et al. 2021.*

A. Clustering of axolotl limb bud scRNA seq expression data reveals six clusters that are readily identifiable by the expression of key markers.

B,C. *Csf1r* and *Arg1* label two macrophage clusters in the axolotl blastema scRNA seq dataset.

D. *Prrx1* labels mesenchymal cells in the axolotl blastema scRNA seq dataset.

E. *Krt12* labels epidermal cells in the axolotl blastema scRNA seq dataset.

F. *Cdh5* labels endothelial cells in the axolotl blastema scRNA seq dataset.

G. *Hbz* labels blood cells in the axolotl blastema scRNA seq dataset.

Supplementary Figure 3.

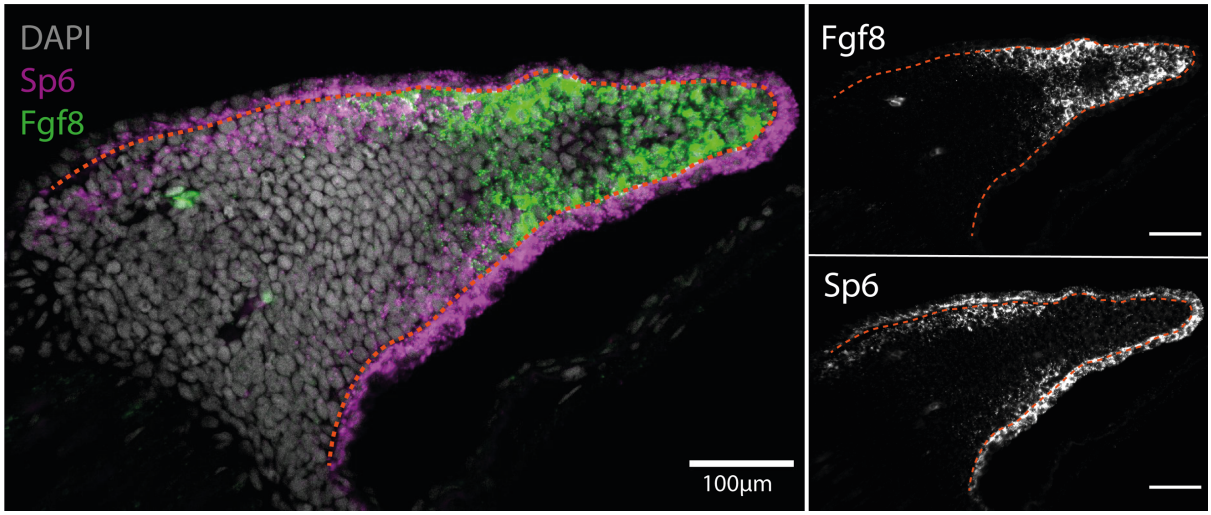

Supplementary Figure 3. *Sp6* is expressed in the basal epidermis and proximal mesenchyme in the axolotl limb bud (n=4).
A. Single plane image from a whole mount limb bud HCR staining of *Sp6* and *Fgf8* transcripts.
B. *Fgf8* expression is localized to the distal mesenchyme of the axolotl limb bud.
C. *Sp6* is ubiquitously expressed in the epidermis but only expressed in the proximal mesenchyme of the axolotl limb bud.
Dashed lines demarcate epidermal-mesenchymal boundaries.

Supplementary Figure 4.

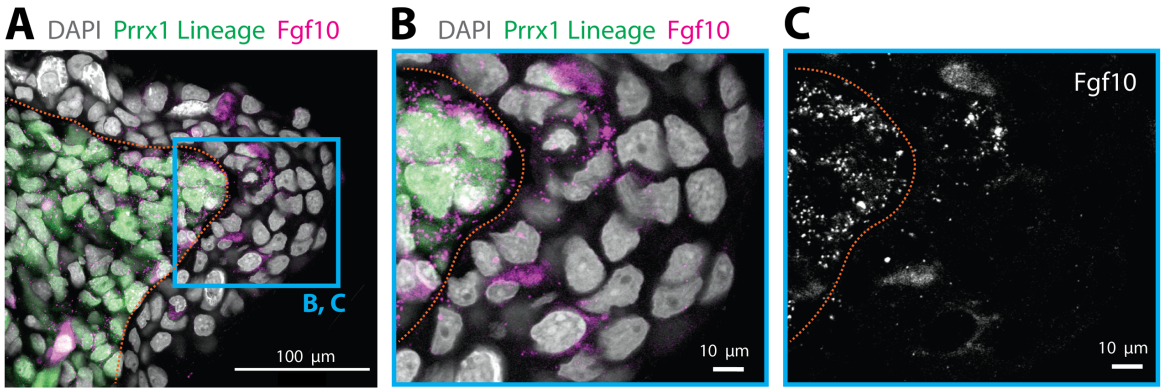

Supplementary Figure 4. Epidermal cells expressing *Fgf10* are not of mesenchymal origin
A. *Fgf10* transcripts are present in epidermal cells that are not *Prrx1* lineage labelled in the axolotl blastema. *Fgf10* transcripts are present in epidermal cells that are not *Prrx1* lineage labelled in the axolotl blastema (n=4 blastemas). HCR in situ hybridization performed in a tissue section of a *Prrx1:Cre-ER;CAGGs:lp-Cherry* animal that was tamoxifen converted during limb development. Green cells are cells of mesenchymal lineage origin.
B, **C.** Magnifications of the box outlined in A.
Dashed lines demarcate epidermal-mesenchymal boundaries.

Supplementary Figure 5.

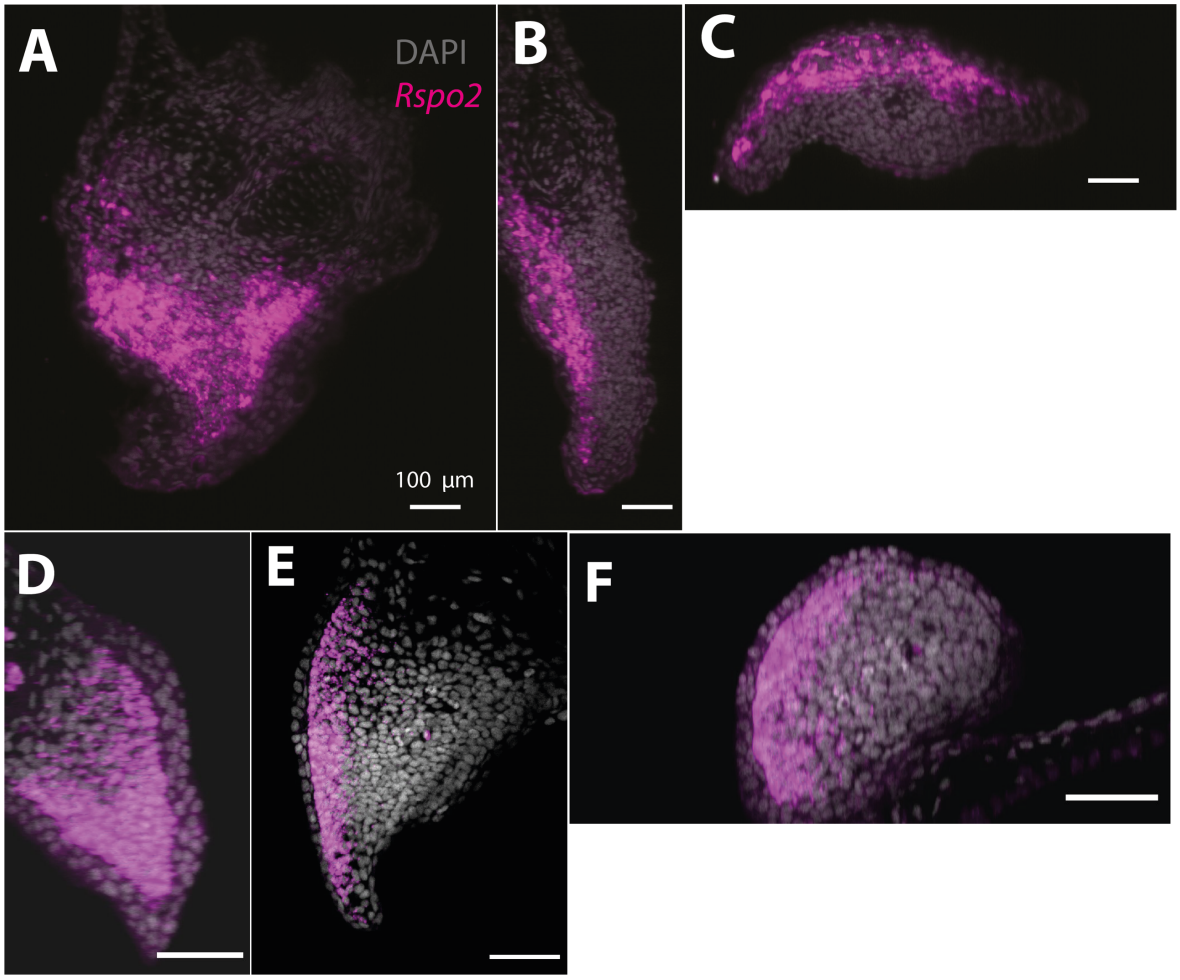

Supplementary Figure 5. *Rspo2* expression is biased along the dorso-ventral axis in the axolotl blastema (A, B, C) and limb bud (D, E, F) (n=4)
A. Single plane image from a whole mount blastema HCR staining of Rspo2 transcripts.
B. Cross section of the blastema proximo-distal axis showing biased expression along the dorso-ventral axis.
C. Cross section of the blastema anterior-posterior axis showing biased expression along the dorso-ventral axis.
D. Single plane image from a whole mount limb bud HCR staining of Rspo2 transcripts.
E. Cross section of the limb bud proximo-distal axis showing biased expression along the dorso-ventral axis.
F. Cross section of the limb bud anterior-posterior axis showing biased expression along the dorso-ventral axis.

Supplementary Figure 6.

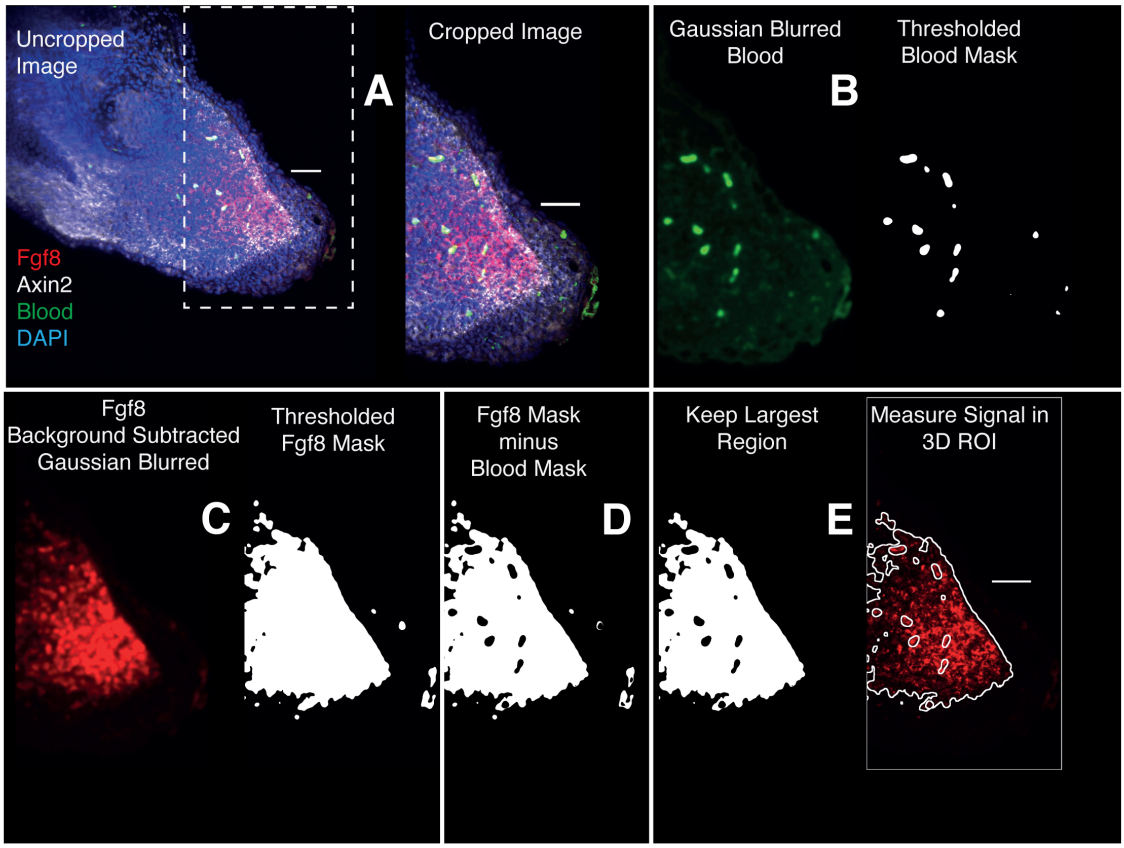

Supplementary Figure 6. Image analysis workflow for whole mount HCR signal quantification inside gene expression domains

A. 3D images are cropped distal to the amputated bone.

B. The Image acquired using 488 illumination (no HCR staining) is used to generate a 3D mask of the auto-fluorescent blood cells. The mask is generated by thresholding after denoising (Gaussian Blur).

C. HCR images are background subtracted, denoised and thresholded to generate a mask containing HCR signal + autofluorescence.

D. HCR signal is isolated subtracting the previously obtained autofluorescence mask from the gene expression mask.

E. The resulting mask is refined and used for 3D signal quantification.

Supplementary Figure 7.

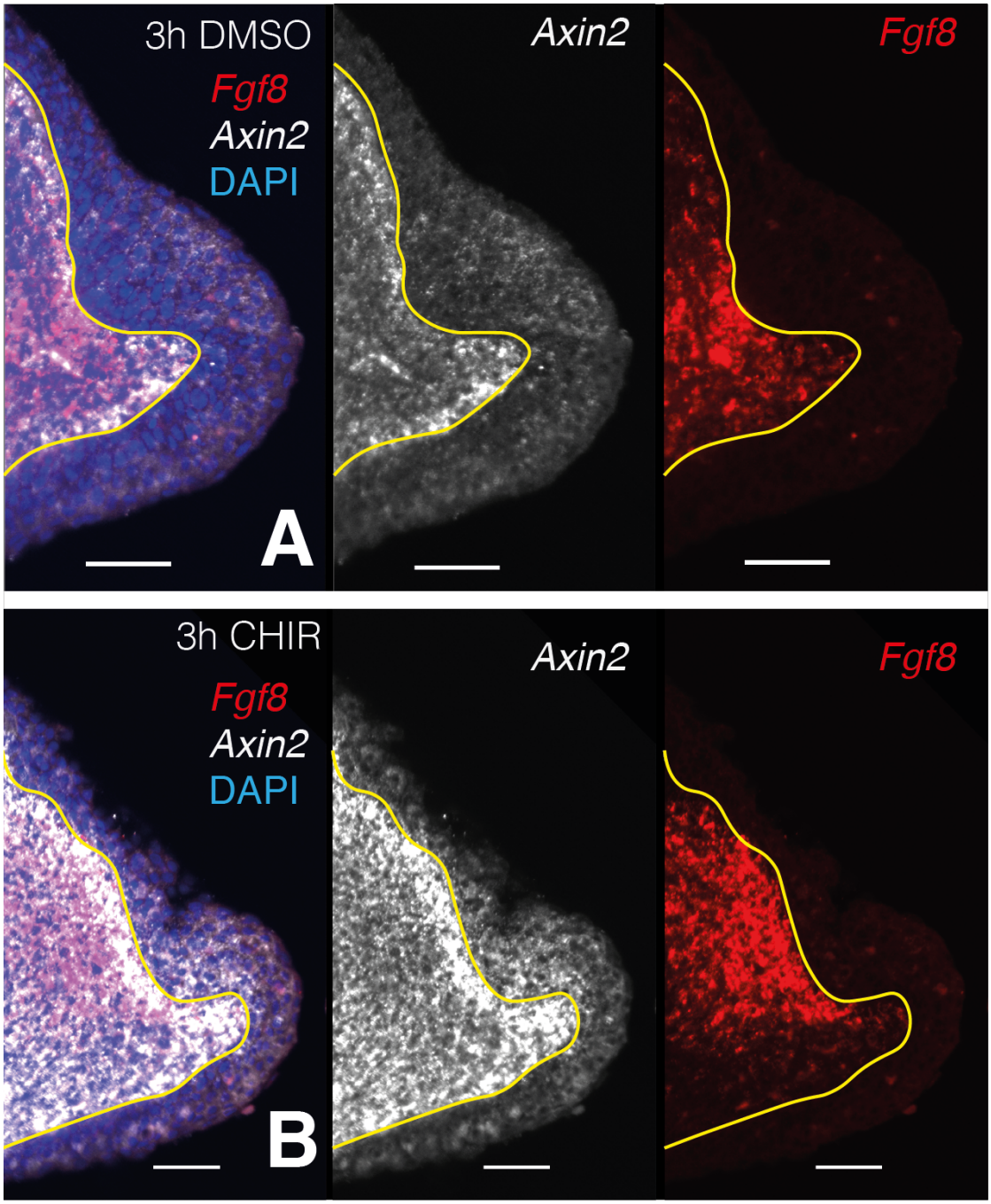

Supplementary Figure 7. Single plane images from whole mount stacks of 3 hours CHIR-treated and DMSO-control samples.
A. 3 hours DMSO control blastema. From left to right: composite multichannel image, *Axin2* alone, Fgf8 alone.
B. 3 hours CHIR treated blastema. From left to right: composite multichannel image, *Axin2* alone, *Fgf8* alone.
A,B. All pairs from treated and control are displayed with the same settings.
Yellow lines demarcate epidermal-mesenchymal boundaries.

Supplementary Figure 8.

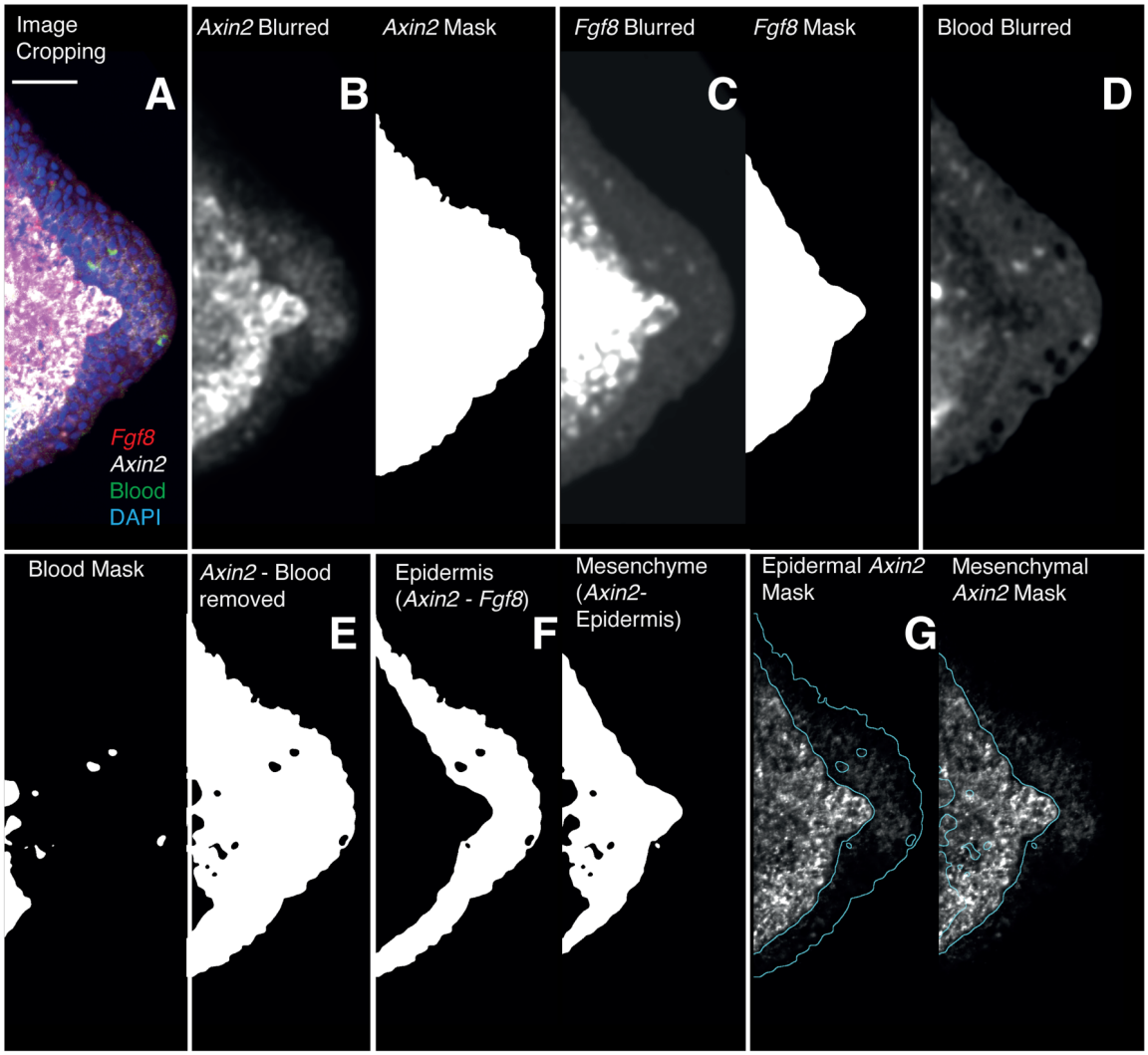

Supplementary Figure 8. Image analysis workflow for the quantification of *Axin2* HCR signal quantification in the epidermal and mesenchymal domains.
A. 3D images are cropped, in the cropped images the entire mesenchyme contains *Fgf8* transcripts. **B,C.** HCR images for *Axin2* and *Fgf8* are denoised and thresholded to generate a mask containing HCR signal + autofluorescence. **D.** The Image acquired using 488nm illumination (no HCR staining) is used to generate a 3D mask of the auto-fluorescent blood cells. **E.** The *Axin2* gene expression domain is isolated by subtracting the autofluorescence mask from the previously obtained masks. **F,G.** The *Fgf8* mask is used to outline the mesenchyme. A mask for the *Axin2* epidermal expression domain is obtained subtracting the *Fgf8* mask from the *Axin2* mask. To obtain intensity measurements the 3D masks are applied to the raw data after background subtraction.